

# Impact of Equation of States in Underground Hydrogen and CO<sub>2</sub> storage and Material Balance Analysis

#### **Augusto Celentano**

#### **Supervisors**

Prof. Dario Viberti, Supervisor Dott.ssa Marialuna Loffredo, Co-Supervisor

> Politecnico di Torino October 07, 2025

### **Summary**

The global need to reduce carbon emissions and improve energy security is driving the development of innovative energy production and storage strategies. Depleted Gas Reservoirs (DGRs) represent a significant opportunity for advancing the energy transition. Because these sites offer vast storage volumes and have a proven, natural ability to trap gases, they are highly suitable for two key strategies: Carbon Capture, Utilization, and Storage (CCUS) and building a hydrogen-based economy. For these projects to succeed, however, it is essential to have a precise understanding of how fluids will behave and interact under the high-pressure conditions found deep underground.

This work aims to assess the impact of different Equations of State (EOSs) on the results when simulating underground H<sub>2</sub> and CO<sub>2</sub> storage. Furthermore, a Material Balance Analysis (MBA) using the p/z method is performed in order to evaluate the accuracy of gas storage predictions by comparing the results obtained from the simulator with those derived from MBA. A simplified reservoir model was developed in tNavigator® (Rock Flow Dynamics) which is, to the best of our knowledge, the only one commercial reservoir simulator which has natively implemented the GERG-2008 EOS. The scenarios simulated are the following: first CH<sub>4</sub> production, followed in one case by CO<sub>2</sub> injection and in the other case by H<sub>2</sub>-CH<sub>4</sub> mixtures injection. In the latter scenario three different injection with varying gas composition are simulated: 80% methane + 20% hydrogen, 50% methane + 50% hydrogen and 100% hydrogen. A sensitivity analysis was performed to compare Peng-Robinson (PR), Redlich-Kwong-Soave (RKS) EOS and to quantify the results discrepancy with respect the GERG-2008, which is considered by the technical literature as a reliable and reference model for the prediction of thermodynamic fluids behaviour for wide range of fluids compositions. The main drawback of the GERG-2008 is the relatively high computational time compared to other EOS when it is implemented for compositional reservoir simulation. Constant Composition Expansion (CCE) tests were simulated to assess thermodynamic properties of gas mixtures at reservoir thermodynamic conditions. In particular, the gas compressibility factor (Z-factor) is obtained, and it is essential for applying the material balance method, relevant to evaluate the reservoir performance. However, during the modelling of the gas injection phases a critical issue raised: the CCE tests

is applied to a mixture with constant composition, but during injection, the composition of reservoir fluids changes continuously. Therefore, the CCE method is not able to predict the thermodynamic properties of the gas mixtures during such phase, leaving a critical gap in the ability to perform accurate material balance calculations (p/z analysis) for the injection and storage phases of the project. To overcome this limitation, an analytical method for calculating the Z-factor and gas density during periods of non-constant composition is used. The methodology is based on a reformulation of the real gas law, utilizing analytical expressions for gas density and mixture molar mass. The methodology was validated against production phase data by comparing its results with the outputs from the CCE test. The comparison showed a very low Mean Absolute Percentage Error (MAPE) of less than 1.5% for all tested Equations of State, confirming the accuracy of the approach and supporting its use in the injection stages. Since during the injection, pressure increases, the p/z plot was adapted and allowed to retrieve the Max Injectable Gas (MIG) in volume and mass with low absolute percentage error (APE), compared to simulated data. However, for the hydrogen scenario, the error analysis showed a peak for the case of at 20% of H<sub>2</sub> in the injection stream when using Peng-Robinson EOS, with Absolute Percentage Error (APE) around 5% for both mass and volume estimation. Overall, this study validates an analytical approach to estimate Z-factor from simulation outcomes during injection phase and evaluates the accuracy of the P/z method in prediction the MIG for a given maximum pressure.

### **Contents**

Chapter 1		1
Introductio	n	1
1.1	Underground fluid storage for sustainable supply security	1
1.1	CO <sub>2</sub> storage in depleted gas reservoir	
1.2	H <sub>2</sub> storage in depleted gas reservoir	
Chapter 2		6
	of State	
2.1.	Introduction to Thermodynamic Modelling in	
Engineer	Ş	IXCSCI VOII
2.2.	Overview of EOS	6
2.3	Cubic Equations of State	
2.3	3.1 Definition	
	3.2 Van der Waals	
	3.3 Redlich-Kwong-Soave	
	3.4 Peng-Robinson	
	3.5 Mixing rules	
2.4	GERG	13
	4.1 Helmholtz energy	
2.4	4.2 GERG 2008 EOS	14
Composition	onal Modell	18
3.1	Compositional Modeling in Reservoir Engineering	18
3.2	Black – Oil Model	
3.3	Compositional Model	
3.4	Literature on compositional modelling for UGS	21
Chapter 4		24
-	gy	
4.1	Simulation Set up	24
4.2	Material Balance Analysis	
	2.1 CCE-Based Estimation for the Production Phase	
	2.1 CCE-Based Estimation for the Production Phase 2.2 Development of an Alternative Method for Injection	
	•	
4.3	Computational cost Analysis	32

Chapter 5		34
Results and An	nalysis	34
5.1 Pr	roduction Phase Analysis	34
5.1.1	EOSs Performance	34
5.1.2	Material Balance Analysis	38
5.2 C	O2 Injection Phase Analysis	41
5.2.1	EOSs Performance	41
5.2.2	Material Balance Analysis	44
5.2.3	Computational cost	46
5.3 Hz	2 Injection Phase Analysis	48
5.3.1	EOSs Perfomance	48
5.3.2	Material Balalce Analysis	53
5.3.3	Computational cost	55
Chapter 6		57

### **List of Tables**

Table 1 Reservoir proprierties	25
Table 2 injection scenarios	26
Table 3. GOIP in mass form P\Z from different EOS	39
Table 4 GOIP in mass form P\Z from different EOS	40
Table 5 Pressure vs time for different EOS and Injection scenario	49
Table 6 . Comparison of MGIP in mass and volume for different E	OS during
all H2 injection scenario	53

## **List of Figures**

Figure 1 a) Share of worldwide UGS by regions b) Share of worldwide	le UGS
by storage type in 2010 [3] Errore. Il segnalibro non è de	efinito.
Figure 2 Global CO2 storage projects in DOGRs, which are defined a	s those
that have lost their economic recovery benefits.[6]	3
Figure 3 CO2 capture and geological storage technology [6]	3
Figure 4 An energy system scheme with a underground hydrogen	storage
facility [3]	4
Figure 5 Phase diagram prediction GERG 2008 [15]	15
Figure 6: Overview of the 210 binary combinations that result from	the 21
natural gas components considered for the development of the GERG	G-2008
equation of state.[15]	16
Figure 7 Gas-solubility pressure diagram. [34]	20
Figure 8 CO2 injection dynamic model [38]	22
Figure 9 a) Grid Proprierties b) Strategy	24
Figure 10 Keywords	25
Figure 11 a) Reservoir grid at initial condition b) Reservoir grid	d after
production	26
Figure 12 Well data	26
Figure 13 a) relative permeabilities curve b) corey exponent oil c)	) corey
exponent gas	27
Figure 14 EOS Default parameters a) RKS b) PR c) GERG 2008	28
Figure 15 Gas material balance P/z [34]	30
Figure 16. Comparison of pressures vs time for different EOSs	during
production phase.	35
Figure 17 Current Gas in place Comparison	35
Figure 18 EOS error analysis Production	36
Figure 19. Z-Factor values from CCE output.	37
Figure 20. Z-Factor values calculated with Equation	37
Figure 21. Densities in production phase calculated with equation	37
Figure 22. Densities in production phase retrieved from CCE expe	eriment
simulation	38
Figure 23. (A) Error deviation for Z-Factor. (B) Error deviation for D	ensity.
	38

Figure 24. Comparison of GOIP in volume with P\Z method for different EoS
during production phase
Figure 25. Comparison of GOIP in mass with P\Z method for different EoS
during production phase
Figure 26. Comparison of GOIP in volume from P\Z and simulator during
production phase
Figure 27. Comparison of pressures vs time for different EOSs during Co2
injection phase
Figure 28 Current Gas in place Comparison
Figure 29 EOS error analysis CO <sub>2</sub> Injection
Figure 30. Comparison of calculated densities during CO <sub>2</sub> injection43
Figure 31. Z-Factor from analytical calculation during CO <sub>2</sub> injection43
Figure 32 Matherial balance comparison
Figure 33 Absolute Percentage Error (APE) Between P/Z Method and
Simulator Results for C02 Injection
Figure 34 Computational costs for CO2 injection a) PR b) RKS c) GERG47
Figure 35 Comparison of pressures vs. Time for different EOS during all H2
injection scenario a) H <sub>2</sub> 20% b) H <sub>2</sub> 50% c) H <sub>2</sub> 100%
Figure 36 Current Gas in place comparison a) H2 20% b) H2 50% c) H2 100%
50
Figure 37 EOS Error Analysis a) H2 20% b) H2 50% c) H2 100%50
Figure 38. Comparison of calculated densities for H <sub>2</sub> injection50
Figure 39. Calculated Z-Factor for the 20% H <sub>2</sub> scenario51
Figure 40. Calculated Z-Factor for the 50% H <sub>2</sub> scenario51
Figure 41. Calculated Z-Factor for the 100% H <sub>2</sub> scenario
Figure 42 APE Analysis54
Figure 43 Computational costs for H <sub>2</sub> injection a) 20% b) 50% in molar fraction
55
Figure 44 Computational costs for H <sub>2</sub> injection at 100% molar fraction56

## Chapter 1 Introduction

## 1.1 Underground fluid storage for sustainable supply security

In this work, underground storage in depleted gas reservoir (DGR) of carbon dioxide and hydrogen were both analysed. This choice was not made randomly but has a deep reason. The EU energy strategy is poorly positioned to ensure energy security for the Union, mainly due to its fixation on fossil energy imports. Energy security can holistically be addressed only in case sustainability becomes a priority goal [1].

Following Proedrou's argument, author of the paper "A new framework for EU energy security: putting sustainability first" [1], the EU can best secure its energy supply by focusing on internal changes, such as reorganizing its priorities and fixing market price signals. This approach makes infrastructure for energy storage a vital part of the energy transition. Key elements include upgrading grids and facilities, developing a market for "prosumers" (consumers who also produce energy), and using smart networks to balance renewable sources with user demand. In this context, carbon capture and storage (CCS) helps to quickly lower emissions in hard to abate industries to meet Paris Agreement goals [2]. Meanwhile, hydrogen (H<sub>2</sub>) storage is important for balancing energy needs across seasons, which improves Europe's supply security and independence [3].

The natural geological formation of the continent places Europe as the second worldwide in terms of underground gas storage number of facilities (Figure 1). The number and capacity of underground gas storage facilities have grown consistently in the last 100 years, especially on the continents of the Northern Hemisphere. 642 UGSs were exploited worldwide in January 2010. Most of them were situated in depleted hydrocarbon deposits (476), then in aquifers (82) and in salt caverns (76) [3].

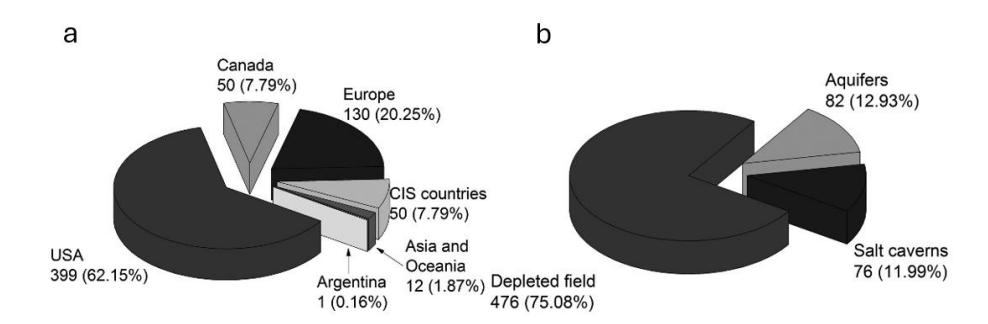


Figure 1 a) Share of worldwide UGS by regions b) Share of worldwide UGS by storage type in 2010 [3].

As major source of infrastructure for UGS, depleted gas reservoir is the first piece of this study.

#### 1.1 CO<sub>2</sub> storage in depleted gas reservoir

CO<sub>2</sub> storage in Depleted Gas Reservoirs (DGR) benefits from the oil and gas industry's extensive knowledge and experience of these systems. The injection of CO<sub>2</sub> into the subsurface has long been a standard practice for Enhanced Oil Recovery (EOR), so the fundamental operational and safety procedures are well-understood. One of the first studies published on CO<sub>2</sub> storage "Confining and abating CO<sub>2</sub> from fossil Fuel burning — a feasible option?"[4] in 1992, was based on experience gained in the oil industry. It should be noted though, that there are two main differences between EOR and CO<sub>2</sub> storage: EOR must be economically viable, i.e. a minimum volume of CO<sub>2</sub> should be injected to obtain a maximum additional oil recovery while some of the CO<sub>2</sub> is produced again with the oil. Conversely, in CO<sub>2</sub> storage projects the maximum volume of CO<sub>2</sub> is injected into the storage site, and all the CO<sub>2</sub> is intended to be stored permanently. For CO<sub>2</sub> storage projects, we are therefore looking at much larger CO<sub>2</sub> volumes than for EOR projects. These differences call for a different approach [5].

However, this existing expertise provides a solid foundation for deploying large-scale storage projects. The worldwide CO<sub>2</sub> storage capacity in DGR is estimated to be around 390-750 gigatons, approximately ten times the current annual CO<sub>2</sub> emissions globally [6]. be around 390-750 gigatons, approximately ten times the current annual CO<sub>2</sub> emissions globally [6].



Figure 2 Global CO2 storage projects in DOGRs, which are defined as those that have lost their economic recovery benefits [6].

Permanent storage, where the goal is to maximize the amount of injected CO<sub>2</sub>, requires a highly accurate compositional model to reliably predict fluid behaviour. This is crucial because the interactions between the CO<sub>2</sub>, residual hydrocarbons in the reservoir and rocks are complex and reservoir specific.

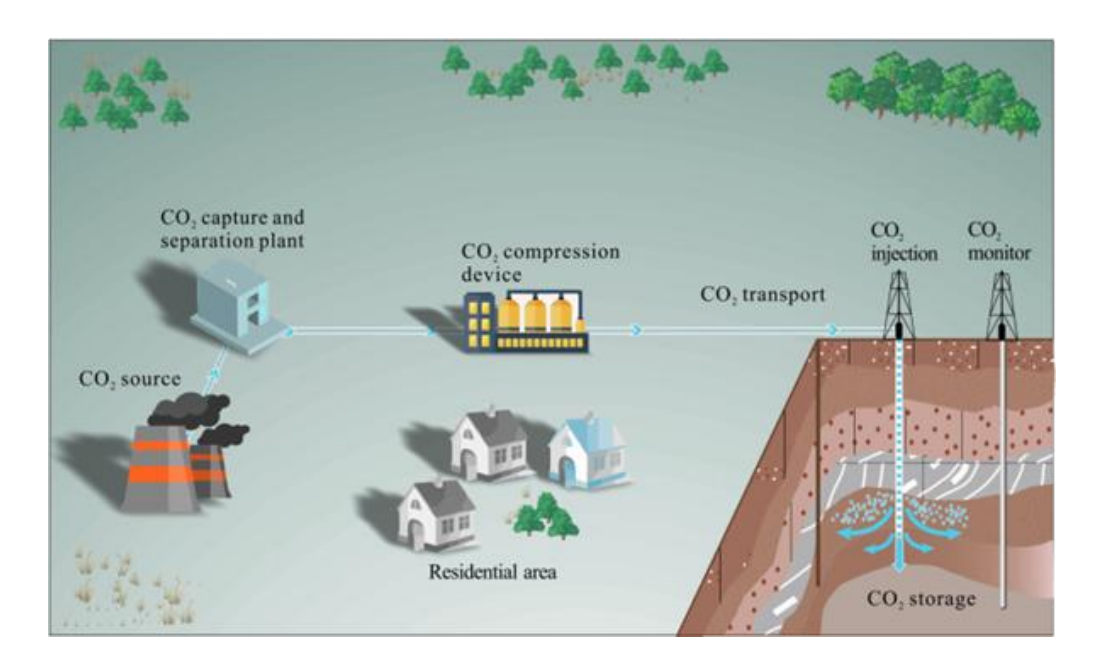


Figure 3 CO2 capture and geological storage technology [6].

An example highlighting the importance of simulation accuracy is the wettability of reservoir rock, a critical property that governs the complex interactions within the CO<sub>2</sub>-rock-water system during geological storage. This single characteristic directly affects crucial outcomes, including CO<sub>2</sub> injectivity, containment security, and the efficiency of both structural and capillary trapping mechanisms [6]. Therefore developing the ability to accurately model this property is essential for creating reliable predictions of CO<sub>2</sub> movement, ensuring long-term storage security,

and maximizing trapping capacity[7]. To reproduce the advantages of a DGR, for this study a primary depletion phase was integrated through a compositional model. This work exploited the knowledge of the depletion phase and used it to get more precise data that could be used for: ensuring the safety permanence of CO<sub>2</sub> in storage site and the amount, generally in tons, of CO<sub>2</sub> possible to be stored.

#### 1.2 H<sub>2</sub> storage in depleted gas reservoir

In the global effort to decarbonize energy systems and meet the ambitious goals of the Paris Agreement [2], renewable sources like wind and solar have become central pillars of the transition. However, their intermittency creates significant challenges in balancing energy supply and demand, necessitating large-scale, long-duration energy storage solutions which exceeds the capability of any surface-based storage facilities. Hydrogen has emerged as an ideal energy carrier for this purpose [8], boasting a high specific energy capacity and clean-burning properties [9] that make it perfect for storing surplus renewable energy and converting it back to electricity when needed.

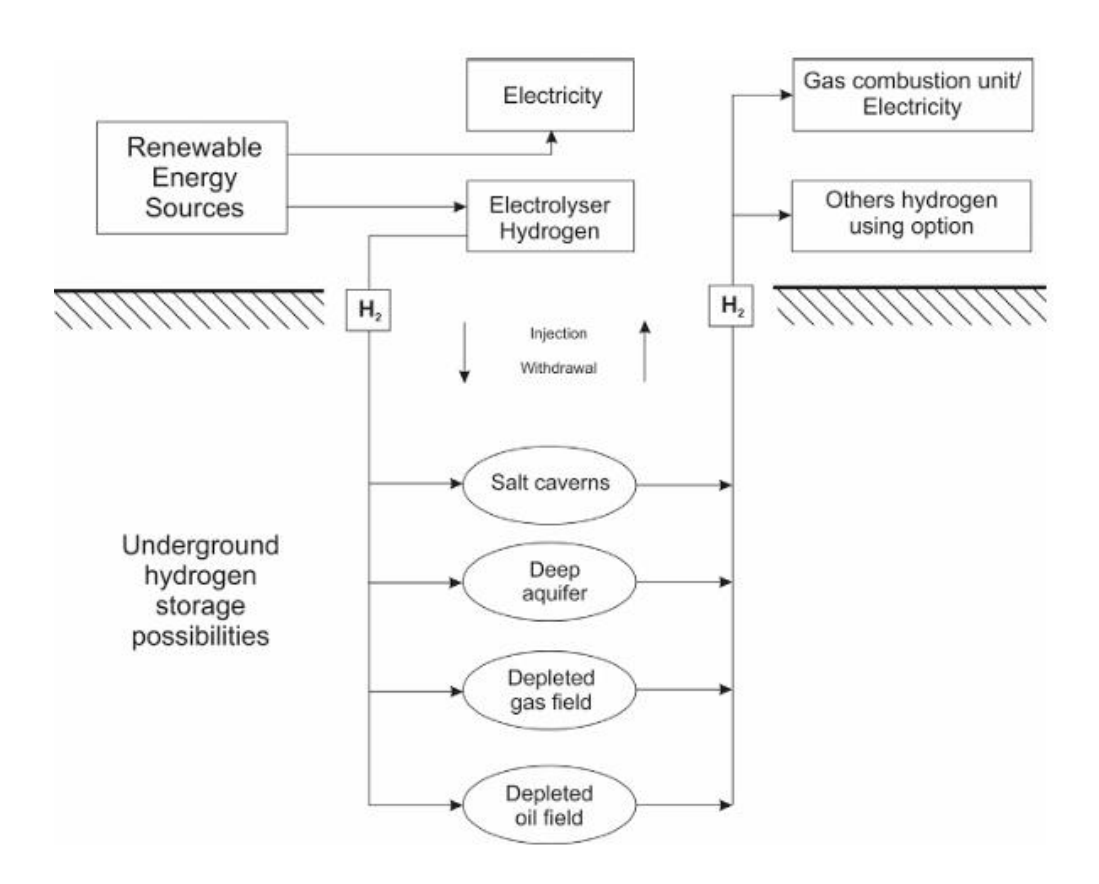


Figure 4 An energy system scheme with a underground hydrogen storage facility [3].

For the gigawatt to terawatt-hour storage capacities required, surface-based facilities are inadequate, making Underground Hydrogen Storage (UHS) in geological formations the only viable path forward [3]. Depleted Gas Reservoirs

are considered one of the most valuable solutions, offering the advantages of validated geological structures, proven cap-rock integrity, and the pre-existence of valuable surface infrastructure. While DGRs provide a promising framework, the operational realities of UHS introduce complexities that require a highly accurate framework for fluid behaviour modelling. A critical operational step in UHS is the use of a cushion gas, such as nitrogen, carbon dioxide, or methane, to maintain reservoir pressure and ensure stable withdrawal rates. However, this practice creates a significant and costly challenge: the inevitable mixing of the injected hydrogen with the cushion gas. Hydrogen, as the lightest and smallest molecule, is highly mobile and diffusive, leading to the formation of a large mixing zone within the reservoir. This mixing directly degrades the purity of the produced hydrogen, requiring additional, energy-intensive separation processes that undermine the economic feasibility of the storage cycle. Simulations that fail to accurately predict the dynamics of this multi-component gas interaction will lead to flawed estimates of recoverable hydrogen purity, operational costs, and overall project viability [10]. Therefore, a model must precisely capture the thermodynamic and transport properties of the specific gas mixtures at reservoir conditions. As mentioned before, a common problem for the underground gas injection is the efficiency of the cap rock to avoid any possible leakage, so the need for accurate fluid property modelling extends far beyond predicting gas mixing. The security and efficiency of UHS are dependent on understanding and quantifying potential hydrogen loss mechanisms, a subject that current simulation tools often oversimplify [10]. Many existing simulators, primarily designed for hydrocarbon recovery, may assume a perfectly impermeable cap-rock for simplicity. This is a dangerous assumption for hydrogen, whose small molecular size makes it capable of leaking through tight rock formations that would easily contain larger molecules like methane. This leakage through the cap-rock represents a direct loss of stored energy and a potential safety concern gap [10].

The aim of this thesis is to evaluate the accuracy of gas storage predictions with material balance calculations and to assess the sensitivity of the EOS used to simulate key H<sub>2</sub> and CO<sub>2</sub> parameters.

## **Chapter 2 Equations of State**

## 2.1. Introduction to Thermodynamic Modelling in Reservoir Engineering

Reservoir fluid properties are important data in the calculation of many aspects of production and reservoir engineering. These properties are critical for efficient reservoir management throughout the life of the reservoir, from discovery to abandonment. Basically, the workflow followed in fluid modelling begins with collecting the samples from the reservoir, analysing the samples and then developing the mathematical models that describe the thermodynamic behaviour of the fluid [11].

#### 2.2. Overview of EOS

Equations of State (EOSs) are fundamental tools in the oil and gas industry, providing a functional relationship between pressure, volume, and temperature to predict the volumetric and phase behaviour of petroleum fluids. Ideally, an EOS should accurately model the volumetric data, vapor-liquid equilibrium (VLE), and thermal properties of a pure substance across the full spectrum of its liquid and gaseous states. Since the pioneering work of Van der Waals in 1873 [12], a multitude of EOSs have been developed, as extensively reviewed in the literature ([13];[14]). The typical development path for these equations involves first formulating them for pure fluids and subsequently extending their application to mixtures through the implementation of mixing rules.

Multiple studies shows that there is that no single, universally applicable EOS that can optimally predict all thermodynamic properties for different types of reservoir fluids. The literature indicates that the effectiveness of an EOS depends on the application [14], [15].

The very beginning of the story is the ideal gas equation:

$$pv = RT, (2.1)$$

where  $v[m^3/kg]$  is the specific volume, R[kJ/kgK] the specific gas constant, where the value depends on the chosen unit, p[Pa] the pressure and T[K] the temperature.

This equation fails when applied to real gas, increasing the divergence from experimental results approaching the critical point The solution was to transform the purely empirical model into a set of empirical and semi-empirical relations by incorporating experimental data.

In 1873 the Dutch physicist Johannes Diderik van der Waals published in a paper [12] the first of the fundamental turning points, presented in the next section, that led to the models used in this work.

According to doctor Diderik the "corresponding state principle" (CSP) govern both pure fluids and mixtures, determining that when compared in terms of dimensionless reduced temperature ( $T_r = T/T_{cr}$ ) and dimensionless reduced pressures ( $p_r = p/p_{cr}$ ), all the real fluid deviate from the ideal behavior approximately in the same manner. Studying the principle in the years two considerations were implemented. In the case we consider determined group of substances similar in molecular constitution the CSP principle can be expressed as two parameter function [14]:

$$p_r = p_r(v_r, T_r), (2.2)$$

Instead, when the constitution is not similar the CSP can be expressed with three parameters, adding at the one of Equation 2.2 the compressibility factor (z) defined as [16]:

$$z = \frac{pv}{RT}. (2.3)$$

Given the critical compressibility factor (Eq. 2.4) and the reduced one (Eq. 2.5):

$$z_C = \frac{p_C v_C}{RT_C},\tag{2.4}$$

$$z_r = \frac{z}{z_C} = \frac{p_r v_r}{T_r}. (2.5)$$

The compressibility factor also can be expressed:

$$z = z_C \frac{p_r v_r}{T_r},\tag{2.6}$$

That way, it is possible to eliminate  $v_r$  from the previous equation to obtain the following 3-parameter relationship where  $z_c$  act as the parameter related to the molecular constitution [17].

$$z = z(T_r, p_r, z_c). (2.7)$$

Experimental results demonstrate this relation fail in presence of high polarized molecules, helium, hydrogen, or neon unless special, modified critical constants are used. An alternative for the third parameter was introduced by Pitzer et al. [18], known as the Pitzer acentric factor ( $\omega$ ). This factor is defined by the following expression at a reduced temperature of Tr = 0.7:

$$\omega = -\log_{10} p_r - 1. \tag{2.8}$$

According to this definition, the acentric factor assumes a value of zero ( $\omega$ =0) for "simple fluids," which Pitzer identified as noble gases like Argon (Ar), Xenon (Xe), and Neon (Ne)[17]. The practical significance of the Pitzer acentric factor is that each substance possesses a unique value that corresponds to its molecular polarity; as the fluid's polarization increases, so does the value of  $\omega$  [18]. For this reason, highly polarized fluids such as water (H<sub>2</sub>O) and ammonia (NH<sub>3</sub>) are characterized by high Pitzer acentric factors. By incorporating this parameter, the 3-parameter Corresponding States Principle (CSP) can be expressed as a function of reduced temperature, reduced pressure, and the acentric factor:

$$z = z(T_r, p_r, \omega) \tag{2.9}$$

#### 2.3 Cubic Equations of State

#### 2.3.1 Definition

Cubic Equations of State (EOSs) are defined as analytical models in which the molar volume is expressed as a third-degree polynomial. This mathematical form is advantageous as it provides closed-form solutions, ensuring computational efficiency. Generally, these equations accurately predict fluid properties for simple, non-polar systems far from critical conditions, but their reliability decreases near the critical point and for highly polar substances [18]. A generalized cubic EOS, building upon the work of Schmidt and Wenzel (1980)[19], was proposed by Daridon et al. (1993) [20] and is expressed as:

$$p = \frac{RT}{v - b} - \frac{a(T)}{v^2 + ubv - wb^2},$$
(2.10)

In this equation, R is the universal gas constant, v is the molar volume, and the parameters a and b are substance dependent. The parameter a is a function of temperature, while b is related to the fluid's critical properties. The temperature dependence of the parameter a is described by the following relationships[21], [22], [23]:

$$a(T) = a_c \alpha(T), \tag{2.11}$$

$$a_c = \Omega_a \left( \frac{R^2 T_C^2}{p_C} \right) \tag{2.12}$$

$$a_c = \Omega_a \left( \frac{R^2 T_C^2}{p_C} \right) \tag{2.13}$$

Here,  $\Omega_a$  and  $\Omega_b$  are dimensionless constants specific to each EOS, and the function  $\alpha(T)$  is an empirical correction factor that improves the model's agreement with experimental data. Physically, the equation's terms represent intermolecular forces: the term  $\left(\frac{RT}{v-b}\right)$  in Equation 2.10, accounts for molecular repulsion, while the term  $\left(\frac{a(T)}{v^2+ubv-wb^2}\right)$  model molecular attraction.

#### 2.3.2 Van der Waals

The first and most straightforward cubic Equation of State was developed by Johannes Diderik van der Waals in 1873[12]. His work represented a significant advancement over the ideal gas law by incorporating terms for both repulsive and attractive intermolecular forces, making it the earliest EOS capable of modelling the coexistence of vapor and liquid phases. The classic Van der Waals expression is given as:

$$\left(p + \frac{a}{v^2}\right)(v - b) = RT. \tag{2.14}$$

When rearranged as a polynomial in molar volume (v), the equation takes its characteristic cubic form:

$$v^{3} - \left(b + \frac{RT}{p}\right)v^{2} + \left(\frac{a}{p}\right)v - \frac{ab}{p} = 0.$$
 (2.15)

This formulation is classified as a cubic EOS due to its third-degree dependency on molar volume. The fluid-specific constants are a, the energy parameter, and b, the co-volume. The  $a/v^2$  term in equation 2.14 introduces a correction for intermolecular attraction, which reduces the pressure relative to an ideal gas. The b parameter accounts for the finite volume of molecules, representing an excluded volume due to repulsive forces. At extremely high pressures, the molar volume approaches the value of b. If both constants are set to zero, the expression simplifies to the ideal gas equation 1.1.

An alternative arrangement, solved for pressure, is:

$$p = \frac{RT}{v - b} - \frac{a}{v^2}. (2.16)$$

The parameters a and b are determined using the thermodynamic conditions at the critical point, where the critical isotherm exhibits a horizontal inflection point.

This is mathematically defined by imposing the first and second derivatives of pressure with respect to molar volume equal to zero at constant temperature:

$$\left(\frac{\partial p}{\partial \nu}\right)_{p_c,\nu_c,T_c} = \left(\frac{\partial^2 p}{\partial \nu^2}\right)_{p_c,\nu_c,T_c} = 0.$$
(2.17)

Applying these conditions to Equation 1.18 we obtain:

$$\left(\frac{\partial p}{\partial v}\right)_{p_c, v_c, T_c} = -\frac{RT_c}{(v_c - b)^2} + \frac{2a}{v_c^3} = 0,$$
 (2.18)

$$\left(\frac{\partial^2 p}{\partial v^2}\right)_{p_c, v_c, T_c} = \frac{2RT_c}{(v_c - b)^3} - \frac{6a}{v_c^4} = 0.$$
 (2.19)

Solving these simultaneous equations provides the expressions for a and b based on critical properties:

$$b = \frac{v_c}{3} = 0.125 \frac{RT_C}{p_C},\tag{2.20}$$

$$a = \frac{9}{8}T_c v_c = 0.4218 \frac{R^2 T_c^2}{p_c}$$
 (2.21)

The EOS can also be formulated in terms of the compressibility factor (z):

$$z^{3} - \left(1 + \frac{pb}{RT}\right)z^{2} + \frac{pa}{R^{2}T^{2}}z - \frac{p^{2}}{R^{3}T^{3}}ab = 0.$$
 (2.22)

From this, the Van der Waals EOS predicts a universal critical compressibility factor of:

$$z_C = \frac{3}{8} = 0,375. \tag{2.23}$$

This predicted value, however, deviates significantly from experimental data for real fluids, which typically show Z<sub>c</sub> values between 0.23 and 0.30 [16]. This discrepancy highlights a major limitation of the Van der Waals equation, especially in accurately describing dense phases. Consequently, this has led to the development of modified, semiempirical cubic EOSs designed to improve the accuracy of the attractive and repulsive terms, particularly in the near critical region. Several different cubic EOS were developed in the years. In the following the two cubic EOSs selected for this study are described.

#### 2.3.3 Redlich-Kwong-Soave

The Redlich–Kwong (RK) equation of state, proposed in 1949 by Redlich and Kwong [24], offered a significant refinement of the Van der Waals model. This modification exclusively targeted the attractive term of the equation, leaving the repulsive part unchanged. It introduced a temperature dependence through the coefficient α, resulting in the following expression:

$$p = \frac{RT}{v - b} - \frac{\alpha(T)a_c}{v(v + b)}.$$
(2.24)

The parameters for this equation are defined as:

$$\alpha = T_r^{-0.5} \,, \tag{2.25}$$

$$a_c = 0.4247 \frac{R^2 T_c^2}{p_c},\tag{2.26}$$

$$b = 0.08664 \frac{RT_c}{p_c}, (2.27)$$

where Tr = T/Tc represents the reduced temperature. Although the RK model was recognized as one of the best two-parameter cubic EOSs for predicting volumetric and thermal properties, it proved to be unsatisfactory for vapor–liquid equilibrium (VLE) calculations. This limitation was attributed to its overly simplistic treatment of the temperature effect, which prevented it from reproducing the vapor pressures of pure substances with sufficient accuracy[25]. To resolve this issue, Soave (1972) [25], developed a new formulation for the temperature-dependent term, known as the  $\alpha$ -function, specifically designed to improve the modelling of vapor pressures:

$$\alpha(T,m) = \left[1 + m\left(1 - \left(\frac{T}{T_c}\right)^{0.5}\right)\right]^2. \tag{2.28}$$

In this expression, the parameter m is correlated with the Pitzer acentric factor ( $\omega$ ), allowing the equation to indirectly account for molecular shape and polarity:

$$m = 0.480 + 1.574\omega - 0.176\omega^2. \tag{2.29}$$

The resulting Soave–Redlich–Kwong (SRK) [25] EOS maintained the original structure of the RK equation:

$$p = \frac{RT}{v - b} - \frac{\alpha(T)a_c}{v(v + b)}.$$
 (2.30)

However, it provided a substantial improvement in the prediction of vapor pressures. As demonstrated by Soave's original work, the SRK EOS significantly reduced the large deviations observed with the RK model, especially for fluids with high acentric factors, and offered an acceptable fit to experimental data. Furthermore, imposing the critical point conditions on the SRK EOS yields a critical compressibility factor of  $Z_c$ =0.33 [25]. While still higher than experimental values for most pure substances, this represented a clear improvement with respect to the Van der Waals equation. Today, the SRK EoS is widely considered a reliable model for hydrocarbons and other non-polar fluids [26].

#### 2.3.4 Peng-Robinson

The Peng-Robinson (PR) EOS is expressed as follows [26]:

$$p = \frac{RT}{v - b} - \frac{a_c \alpha(T)}{v(v + b) + b(v - b)},$$
(2.31)

The parameters  $a_c$  and b for this equation are determined from the fluid's critical properties using these expressions:

$$a_c = 0.45724 \frac{R^2 T_c^2}{p_c},$$
 (2.32)  
 $b = 0.07780 \frac{RT_c}{p_c}.$  (2.33)

$$b = 0.07780 \frac{RT_c}{p_c}. (2.33)$$

While the PR EOS retains an α-function similar in form to the one proposed by Soave, the correlation for the parameter m was refined. This refinement was achieved by equating the fugacities of the coexisting liquid and vapor phases across a temperature range from the normal boiling point up to the critical temperature. This process led to a new empirical relationship for m as a function of the acentric factor ( $\omega$ ):

$$m = 0.37464 + 1.54226\omega - 0.26992\omega^2. \tag{2.34}$$

From this updated formulation, the critical compressibility factor is derived:

$$\frac{p_C}{RT_C} = \frac{z_C}{v} = \frac{1}{v - b} - \frac{\frac{\alpha(T)}{RT_C}}{v^2 + 2bv - b^2}.$$
 (2.35)

This results in a value of z critical  $\approx 0.30$ , which is in much better agreement with the experimentally observed range for real fluids (0.23-0.30) and represents a significant improvement compared to the SRK (Soave-Redlich-Kwong) equation. Comparative studies have confirmed that both the SRK and PR models provide accurate vapor-pressure predictions with small deviations from experimental data, though the Peng-Robinson EOS generally offers slightly better overall performance[27].

#### 2.3.5 Mixing rules

In practical applications, EOS are used on mixtures and not pure components, as most of them were developed for. There are three approaches for extending such equations to mixtures [28]. The first approach involves treating the mixture as a single pseudo-pure substance. This is achieved by calculating a set of effective input parameters for the entire mixture, commonly referred to as pseudocritical properties. The second approach requires determining the necessary properties for each individual component present in the mixture. While this method can yield highly accurate results, it is also computationally demanding. Consequently, its significant computational cost makes it unsuitable for complex mixtures composed of many different components. The third and most widely used approach is based on mixing rules. In this method, the EOS parameters for the mixture are calculated directly by combining the parameters of the individual pure components. This combination is typically weighted by the mole fraction or weight fraction of each component of the mixture, providing a balance between accuracy and

computational efficiency. Peng and Robinson, Redlich and Kwong and Soave used quadratic mixing rule in their papers [24], [25], [26].

$$a = \left(\sum_{i=1}^{N} y_i a_i^{0.5}\right)^2,\tag{2.36}$$

$$b = \sum_{i=1}^{N} yib_i. {(2.37)}$$

This formulation is made for N number of components in the mixture and weighted on the molar fraction of the single component  $y_i$ . Until the mixtures don't contain hydrogen or carbon dioxide great deviations from experimental data are not found [28]. In such case the consideration of binary interaction parameters (BIP), made for specific couples of components, retrieved from experimental data, and suitable only for the EOS for which they are made for, became necessary to fit experimental data.

$$a = \left(\sum_{i=1}^{N} y_i \sum_{j=1}^{N} y_j \, a_{ij}^{0.5}\right)^2,\tag{2.38}$$

$$a_{ij} = (1 - K_{ij})(a_i a_j)^{\frac{1}{2}},$$
 (2.39)

In this form  $K_{ij}$  is the BIP retrieved by minimizing the discrepancy between predicted and experimental data.

#### **2.4 GERG**

#### 2.4.1 Helmholtz energy

Recent advancements in developing equations of state for mixtures are centred on multi-fluid approximations that are explicit in the Helmholtz free energy. These sophisticated models integrate fundamental equations of state for each individual component with specialized correlation equations designed to capture the residual behaviour of the mixture. These equations describe with high accuracy thermodynamic properties, throughout the entire fluid region, including homogeneous gas, liquid, and supercritical states, as well as vapor-liquid equilibrium across extensive ranges of temperature, pressure, and composition. The development and validation of these empirical models are based on experimental data [29].

In this approach, the total Helmholtz free energy a is decomposed into an ideal part  $a^0$ , representing the properties of an ideal-gas mixture, and a residual part  $a^r$ , which accounts for real-fluid behavior:

$$a(\rho, T, \mathbf{x}) = a^0(\rho, T, \mathbf{x}) + a^r(\rho, T, \mathbf{x}). \tag{2.40}$$

For practical implementation, the equation is expressed in a dimensionless form using the reduced Helmholtz free energy:

$$\alpha(\delta, \tau, \mathbf{x}) = \alpha^{o}(\rho, T, \mathbf{x}) + \alpha^{r}(\delta, \tau, \mathbf{x}). \tag{2.41}$$

Here,  $\delta$  is the reduced mixture density and  $\tau$  is the inverse reduced mixture temperature, defined as:

$$\delta = \frac{\rho}{\rho_r},\tag{2.42}$$

$$\tau = \frac{T_r}{T'},\tag{2.43}$$

where:

$$\rho_r = \rho_r(\mathbf{x}),\tag{2.44}$$

$$T_r = T_r(\mathbf{x}). \tag{2.45}$$

are composition reducing functions. The dimensionless Helmholtz free energy for the ideal gas portion of the mixture,  $\alpha^o$ , is given by:

$$a^{o}(\rho, T, \mathbf{x}) = \sum_{i=1}^{N} x_{i} [\alpha_{oi}^{o}(\rho, T) + lnx_{i}].$$
 (2.46)

In this expression, N is the number of components,  $\alpha_{oi}^o$  is the ideal-gas contribution of component i, and the logarithmic term accounts for the entropy of mixing. The residual part of the reduced Helmholtz free energy,  $\alpha^r$ , is calculated within the multi-fluid approximation as:

$$\alpha^{r}(\rho, T, \mathbf{x}) = \sum_{i=1}^{N} x_{i} \alpha_{oi}^{r}(\delta, \tau) + \Delta \alpha^{r}(\delta, \tau, \mathbf{x}).$$
 (2.47)

This term is composed of two distinct parts: a linear combination of the residual parts of all pure components  $\alpha_{oi}^r$ , and a departure function  $\Delta \alpha^r$ . The departure function corrects for the non-ideal interactions between different molecules in the mixture and generally provides a smaller contribution to the total residual energy than the sum of the pure component parts. The development of a robust mixture model based on the multi fluid approximation however necessitates an EOS that accurately predicts the behaviour of each individual component and then of the departure function that depends on the mixture properties. This need to be coupled with a reducing function, specifically defined, for the mixture reducing density and temperature [30].

#### 2.4.2 GERG 2008 EOS

The GERG Equation of State, developed by the Gas Research Group, is a highly advanced thermodynamic model for predicting the properties of natural gas and

other multicomponent mixtures. Unlike traditional cubic models like Peng-Robinson or Soave-Redlich-Kwong, the GERG EOS is based on a multi-fluid approximation and an explicit Helmholtz free energy formulation. This sophisticated structure allows it to reproduce experimental data with high accuracy across wide ranges of temperature, pressure, and composition. Consequently, the GERG EOS has become the benchmark model for the natural gas industry, particularly in applications requiring high precision, such as modelling of complex gas blends [15].

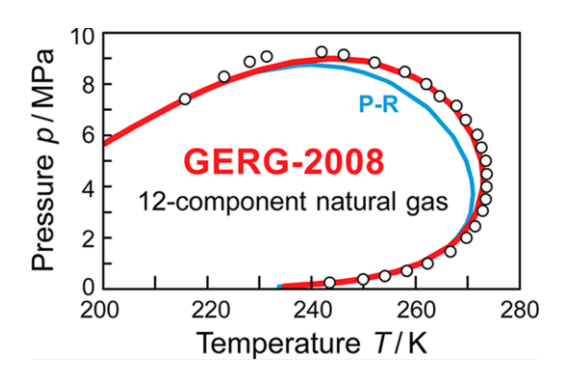


Figure 5 Phase diagram prediction GERG 2008 [15]

The model's development occurred in stages. The initial version, GERG-2004 [29], was formulated for 18 components typically found in natural gas, combining accurate EOSs for each pure fluid with empirically derived functions for their binary interactions parameters. The subsequent GERG-2008 [15] version expanded the component list to 21 (adding n-nonane, n-decane, and hydrogen sulfide), thereby increasing the number of considered binary systems to 210. This extension allowed for the accurate modelling of a broader range of gas compositions, including those with heavier hydrocarbons and sulphur compounds. The formulation of such an empirical Equation of State relies on experimental data that are used to determine the structures, coefficients, and parameters of the correlation equations and to evaluate the behaviour of the equation of state in different fluid regions.

The theoretical foundation of the GERG-2008 model is the decomposition of the reduced Helmholtz free energy a of a mixture into an ideal  $\alpha^o$  and a residual contribution  $\alpha^r$ . The residual part, which accounts for real-fluid behaviour, is further broken down into contributions from the pure substances and from the binary interactions between them:

$$\alpha^{r}(\delta, \tau, \mathbf{x}) = \sum_{i=1}^{N} x_{i} \alpha_{oi}^{r}(\delta, \tau) + \sum_{i=1}^{N-1} \sum_{j=i+1}^{N} x_{i} x_{j} F_{ij} \alpha_{ij}^{r}(\delta, \tau),$$
(2.48)

where  $\delta$  is the reduced mixture density and  $\tau$  is the inverse reduced mixture temperature according to Eq. 2.44 and Eq. 2.45 respectively and N is the total

number of components in the mixture. Eq. 2.48 considers the residual behavior of the mixture at the reduced mixture variables  $\delta$  and  $\tau$ . The first sum in this equation is the linear contribution of the reduced residual Helmholtz free energy of the pure substance equations of state multiplied by the mole fractions  $x_i$ . The double summation in Eq. 2.48 is the departure function  $\Delta \alpha^r(\delta, \tau, \mathbf{x})$ , which is the summation over all binary specific and generalized departure functions  $\Delta \alpha^r_{ij}(\delta, \tau, \mathbf{x})$  developed for the respective binary mixtures.

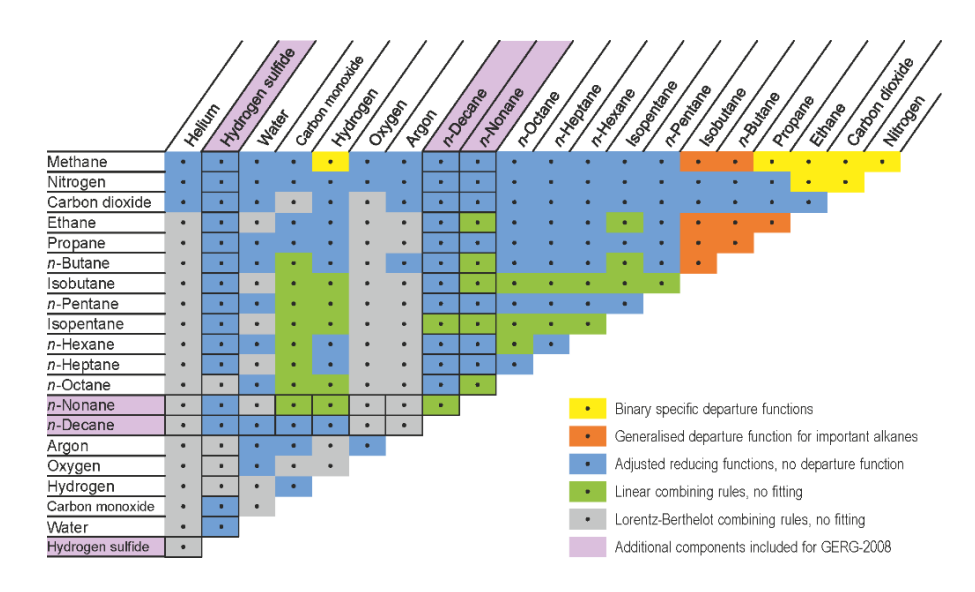


**Figure 6** Overview of the 210 binary combinations that result from the 21 natural gas components considered for the development of the GERG-2008 equation of state[15].

Figure 6 provides a visual overview of the 210 binary combinations that form the basis of the GERG-2008 equation of state, which models 21 natural gas components [15]. It specifically highlights the 57 new binary mixtures that were introduced after the GERG-2004 version by adding three new components: n-nonane, n-decane, and hydrogen sulfide (in pink). The diagram uses a color-coded system to explain the specific modeling approach used for each pair:

- Yellow and Orange Fields: For these mixtures, a specific departure function was fitted to experimental data, and the parameters of the reducing functions were also fitted.
- Blue Fields: In these cases, only the parameters of the reducing functions were fitted to experimental data.
- Green and Gray Fields: These indicate mixtures where standard combining rules were applied to the reducing functions without any fitting to experimental data.

The GERG-2008 equation of state demonstrates exceptional accuracy across a wide range of applicability. The model's normal validity range covers temperatures from 90 to 450 K and pressures up to 35 MPa, with an extended range reaching up to 700 K and 70 MPa. Within this scope, its uncertainty in gas-phase density is remarkably low, at approximately 0.1% for temperatures between 250 and 450 K and pressures up to 35 MPa [15]. This proven high fidelity has established GERG-2008 as the

industry standard for generating benchmark or "ground truth" data. For this reason, in this thesis, the results obtained from the Peng-Robinson (PR) and Soave-Redlich-Kwong (SRK) equations are evaluated by comparing them directly against the reference data produced by the GERG-2008 model.

## **Chapter 3 Compositional Modell**

#### 3.1 Compositional Modeling in Reservoir Engineering

For displacement processes that are sensitive to changes in pressure and fluid composition, an Equation of State (EOS) is required to accurately simulate both the equilibrium transfer between and fluid's mass phases the Pressure/Volume/Temperature (PVT) behaviour. While laboratory **PVT** measurements typically cover only a limited segment of the compositional path, an EOS can predict fluid behaviour across the full range of compositions and pressures experienced during the process. Numerous field development projects are strongly dependent on compositional effects, including the production from gas/condensate reservoirs, enhanced oil recovery methods like miscible gas injection or wateralternating-gas (WAG) injection [31], large-scale modelling to evaluate the behaviour of the injected CO<sub>2</sub> in various scenarios [32] and evaluate the feasibility of UHS in DGR [10]. Historically, the industry relied on simplified methods like black-oil models or limited-composition simulators to approximate this complex phase behaviour. These approaches were selected due to the lower computational time and reduced memory requirement, making them suitable for quick, preliminary performance evaluations. However, significant advancements in parallel computing hardware and software over the last several years, driven by efforts from both industry and academia, have increased simulation efficiency. These improvements have now made full compositional simulation a practical and accessible tool for modern reservoir management [31].

#### 3.2 Black – Oil Model

The black-oil model is a simplified three-phase reservoir fluid model in which water is modelled explicitly alongside two hydrocarbon components: a pseudo-oil phase and a pseudo-gas phase. In this formulation, all hydrocarbons produced are assumed to separate into fixed stock-tank oil and dry gas components at surface

conditions, and the reservoir fluids are treated as combinations of these two hydrocarbon pseudo-components.

The TOIL\_IMS module within PFLOTRAN, an open-source subsurface simulator, offers a clear illustration of the fundamental structure of a black-oil type model[33]. This module is designed to simulate non-isothermal, immiscible oil-water flow, and its mathematical framework is built upon three primary governing equations:

$$\frac{\partial}{\partial t}(\phi s_{\alpha} \eta_{\alpha}) + \nabla \cdot (\eta_{\alpha q_{\alpha}}) = Q_{i} \tag{3.49}$$

$$\frac{\partial}{\partial t} \left[ \Phi \sum_{\alpha} s_{\alpha} \eta_{\alpha} U_{\alpha} + (1 - \Phi) \rho_{r} c_{r} T \right] + \nabla \cdot \left[ \sum_{\alpha} \eta_{\alpha q_{\alpha}} H_{\alpha} + \kappa \nabla T \right] = Q_{e}; \quad (3.50)$$

$$q_{\alpha} = \frac{Kk_{\alpha}}{\mu_{\alpha}} \nabla (P_{\alpha} - \rho_{\alpha}gz). \tag{3.51}$$

These equations are a molar balance equation (Equation. 3.49), which is equivalent to a mass balance, applied to each fluid phase (oil and water), a single energy conservation equation is used, which assumes thermal equilibrium between the fluid phases and the rock and neglects kinetic and potential energy effects (Equation 3.50) and a fluid flow equation Darcy's law is implemented to describe the flux of each individual phase through the porous medium (Equation 3.51). This opensource implementation effectively demonstrates the core principles of black-oil modelling, where the conservation of mass and energy, coupled with Darcy's law, provides the complete description of reservoir flow [33]. The model assumes instantaneous thermodynamic equilibrium between the oil and gas in each grid cell, meaning that at a given cell the oil can be either saturated (dissolved gas at its bubble-point pressure with free gas present) or undersaturated (no free gas, with reservoir oil holding less gas than its capacity). The oil-water-gas system is parameterized using three primary variables. The specific choice of these variables depends on the fluid state: one set is used for saturated conditions (where a free gas phase exists), and another for undersaturated conditions. A state variable is therefore maintained for each grid cell to switch between these two formulations as needed. The quantity of dissolved gas is described by the solution gas-oil ratio or solubility (Rs), defined as the number of standard cubic feet of gas that will dissolve in one stock-tank barrel of crude oil at certain pressure and temperature [34].

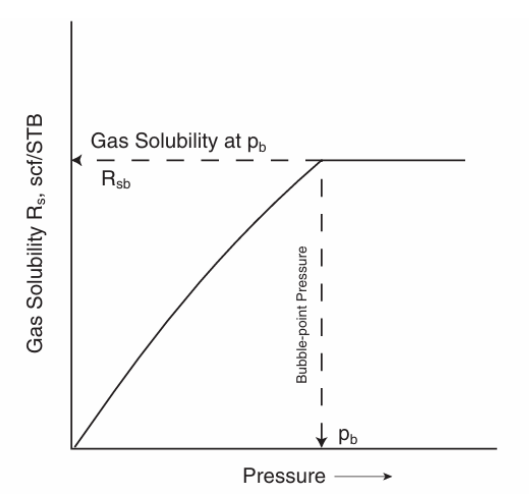


Figure 7 Gas-solubility pressure diagram [34]-

Key oil properties, such as the formation volume factor (Bo), viscosity, and enthalpy, are then treated as functions of pressure and the bubble point pressure.

#### 3.3 Compositional Model

The mathematical basis of a compositional model is a set of mass conservation equations, with one equation for each of the N. hydrocarbon components plus an additional equation for water. To ensure stability when dealing with strong nonlinearities and to allow for large time steps, this coupled system of conservation equations is typically solved using a fully implicit formulation. Each conservation equation quantifies the accumulation, transport, and source/sink terms for a specific component [35]. The transport of each component is described by Darcy's law, which incorporates the effects of viscous, gravitational, and capillary forces. Crucially, these flow equations are solved simultaneously with thermodynamic equilibrium constraints, ensuring that the fluid phases are consistent and in equilibrium within every grid block of the reservoir model at each time step.

The core of the phase behaviour description is an Equation of State (EOS), with the most commonly used being cubic equations such as the Peng–Robinson (PR)[26] or Soave–Redlich–Kwong (SRK) [25] models. The EOS is used to calculate critical fluid properties, including the fugacities, densities, and equilibrium ratios (K-values) for each phase. For example, the PR EOS [26] is typically used to determine the densities and fugacities of the oil and gas phases, while specialized mixing rules, like the Wong–Sandler model [36], may be applied to adjust for water–hydrocarbon interactions. To calculate fluid viscosities, simulators generally use semi-empirical correlations, with the Lohrenz–Bray–Clark method [37] being a very common choice. When this type of transport model is used together with thermodynamic models, the simulator can accurately represent the complex interactions between components as they move from one phase to another under changing pressure and

temperature. A core assumption for many compositional models is that instantaneous thermodynamic equilibrium exists within each grid cell. This means that for any single component, its fugacity value in the oil phase is assumed to be equal to its fugacity value in the gas phase. This condition is what ensures the correct distribution of components between the different phases [35]. A common simplification is applied when dealing with the aqueous phase in the model. This involves treating only specific components, such as CO<sub>2</sub> and sometimes H<sub>2</sub>S, as capable of dissolving in both the water and hydrocarbon phases. This approach is justified for two reasons: it reflects the much higher solubility of CO2 in water compared to other hydrocarbons, and it reduces the overall computational workload. The related principle of equal fugacity is critical for processes like CO<sub>2</sub> flooding and storage. This constraint ensures the model correctly calculates the partition between dissolved CO<sub>2</sub> and free CO<sub>2</sub>, providing a result that is thermodynamically consistent [35]. A key advantage of compositional simulation is its capacity to precisely model processes that are governed by thermodynamic principles, such as the development of miscibility and multiple-contact displacement. This makes it a particularly effective tool for predicting reservoir performance in situations where gas injection causes major changes to the fluid composition, or during the underground storage of hydrogen and CO<sub>2</sub> [9]. These processes are driven by strong compositional effects that cannot be adequately captured by empirical black-oil approximations. Furthermore, compositional models provide access to unique, component-specific outputs, such as the partitioning of CO<sub>2</sub> between the aqueous and hydrocarbon phases, which is essential information for many environmental and industrial applications [31].

#### 3.4 Literature on compositional modelling for UGS

Recent research highlights the critical role of compositional reservoir simulation in evaluating the feasibility of Underground Hydrogen Storage (UHS) in depleted gas reservoirs. One such study utilized the TOUGH + RealGasBrine (T+RGB) [10] simulator to model the complex phase behaviour of hydrogen-hydrocarbon-water systems. A key part of the methodology involved calibrating several Equations of State, with the Soave–Redlich–Kwong EOS ultimately being selected for its optimal balance of accuracy and computational efficiency. The compositional model successfully captured the displacement of methane by injected hydrogen, revealing significant gravity segregation effects that concentrated hydrogen at the top of the reservoir. The simulations quantified hydrogen loss mechanisms, showing that leakage into the cap rock was minimal (<0.05%) for typical cap-rock permeabilities, and dissolution into the aqueous phase was low (~1%). However, the study found that recovery efficiency was limited, with a maximum of 73% of the injected hydrogen being recoverable under the simulated production conditions.

This finding highlights the necessity of using cushion gas, such as nitrogen or CO<sub>2</sub>, to improve pressure support and overall storage performance. Overall, with this work Tianjia Huang and George J. Moridis [10] demonstrates that EOS-based compositional simulation is essential for quantifying key operational parameters like storage efficiency and leakage risk, providing a benchmark for designing future large-scale UHS projects.

A significant advancement in compositional simulation for Carbon Capture, Utilization, and Storage (CCUS) is the integration of the GERG-2008 Equation of State into dynamic reservoir models. While GERG-2008 has long been the industry standard for high-accuracy static PVT calculations of CO<sub>2</sub>-rich mixtures, its use in field-scale dynamic simulation has been limited, creating a gap between laboratory-grade accuracy and practical reservoir modelling.

The cited study [38] bridges this gap by embedding the GERG-2008 EOS within a dynamic reservoir simulator specifically designed for CCUS projects. Comparative simulations were conducted to benchmark the performance of GERG-2008 against traditional cubic models, such as the SRK and PR equations. The findings demonstrate that GERG-2008 provides consistently superior predictions, particularly in modelling the behaviour of supercritical CO<sub>2</sub> and its associated heat exchange parameters. This enhanced accuracy is critical for simulating conditions above CO<sub>2</sub>'s critical point (73.8 bar and 31.1 °C), where its unique fluid properties govern storage behaviour.

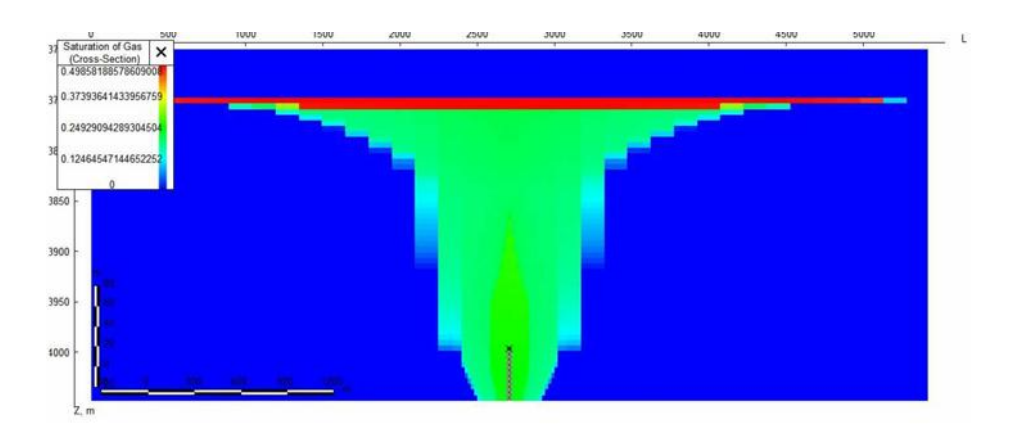


Figure 8 CO2 injection dynamic model [38]

A key outcome of this work is that the use of GERG-2008 not only improves the fidelity of thermophysical property predictions but also enhances the stability and safety margins of storage forecasts. The ability to reliably model the supercritical state is essential for accurately predicting CO<sub>2</sub> plume migration, ensuring caprock integrity, and evaluating long-term storage performance. In conclusion, incorporating the GERG-2008 EOS into dynamic simulators represents a major

methodological step forward for compositional CCUS modelling, leading to more reliable designs and security assessments for CO<sub>2</sub> storage projects in geological formations. Given that the objective of this work is to evaluate the performance of different EOS, in particular PR, RKS, GERG-2008, in simulating CO<sub>2</sub> and H<sub>2</sub> underground storage.

## Chapter 4 Methodology

#### 4.1 Simulation Set up

A simplified reservoir model was built using tNavigator. Figure 9 a) shows the interface to define grid proprieties that are reported in table 1. After imposing the entire reservoir as one equilibration region the datum and the pressure at datum depth were chosen at 2500 m and 250 bar. To give properties of porous medium to the cell of the grid such as porosity, absolute permeability and net to gross (table 1), different keywords were used (Figure 10). The temperature of reservoir was set constant at 50°C.

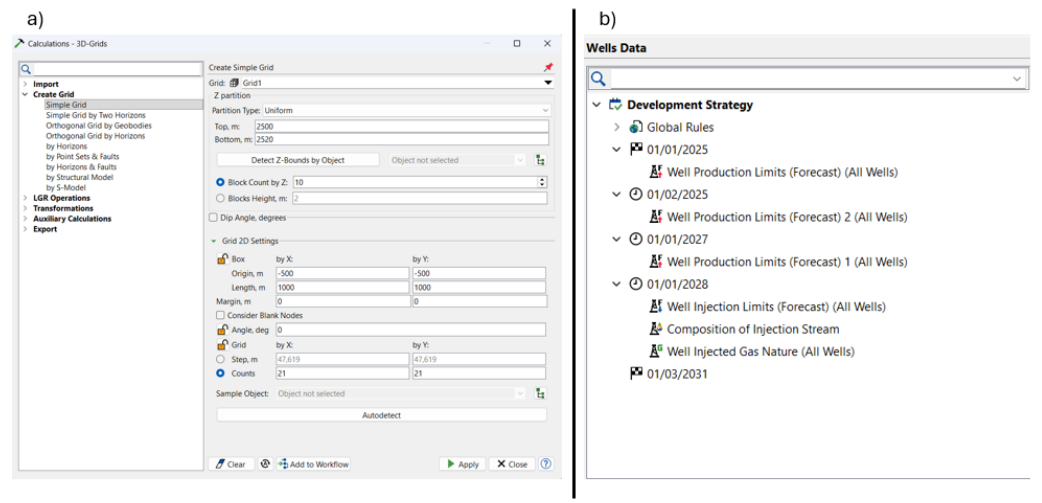


Figure 9 a) Grid Proprierties b) Strategy

#### Methodology

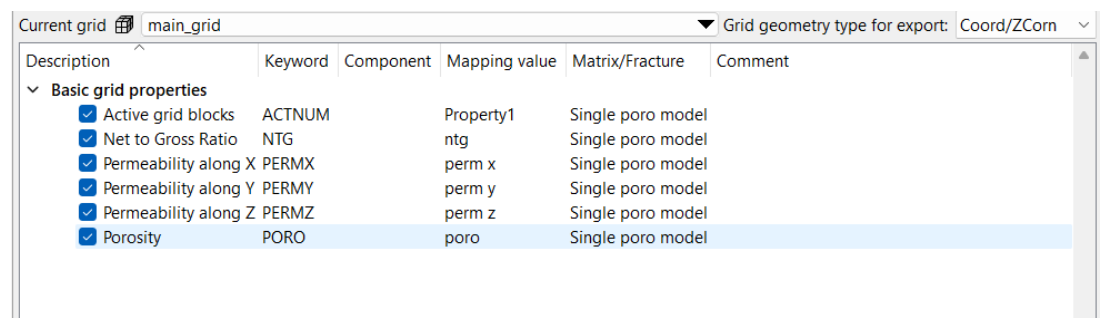


Figure 10 Keywords

Table 1 Reservoir proprierties

Table 1 Reservoir proprierties			
Parameter	Value		
Reservoir dimension [m]	1000 X 1000		
Layer Thickness [m]	20		
Grid resolution [cells]	21X21		
Number of vertical layers	5		
Depth [m]	2500		
Porosity [%]	20		
Net to Gross Ratio [%]	100		
Swirr [%]	20		
Kabs along x, y and z. [mD]	100		

Only one well was placed in the reservoir and the characteristics are reported in Figure 12. Once the Reservoir structure and proprieties were defined (Figure 12a), a strategy was imposed (Figure 9 b)). From 01/01/2025 to 01/02/2025 the option Well Production limit (Forecast) was used to set a first month of shut in. From 01/02/2025 to 01/01/2027 the production start with a constant rate of 1000000 m3/day and with a lower pressure limit of 50 bar. This make the simulator started decreasing the rate as limit lower pressure approached. From 01/01/2027 to 01/01/2028 a shut in period was imposed. The last part of the strategy involves the injection phase from 01/01/2028 to 01/01/2031, where the option Composition of Injection Stream allows us to choose a gas rate with a specific molar mixture. While the first stage of production is constant in all the scenario, 4 different scenarios are simulated changing the injection

composition (table 2) with a constant volumetric rate of 1000000 m<sup>3</sup>sc/day.

Table 2 injection scenarios

Scenario	Molar percentage	Molar percentage	Molar percentage
Scenario	CH <sub>4</sub>	$CO_2$	$H_2$
1	-	100%	-
2	80%	-	20%
3	50%	-	50%
4	-	-	100%

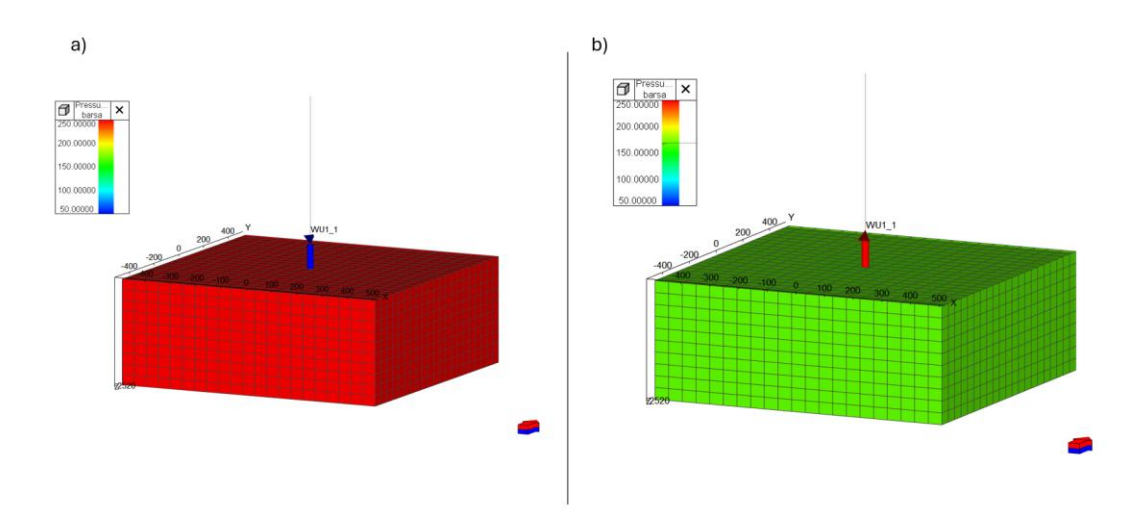


Figure 11 a) Reservoir grid at initial condition b) Reservoir grid after production

	Well	Date	Event	Top, m	Bottom , m	Depth	Diameter, m
1	WU1_1 →	01/01/2025	Perforation 🕶	2500	2520	MD +	0,16
	Type or paste						

Figure 12 Well data

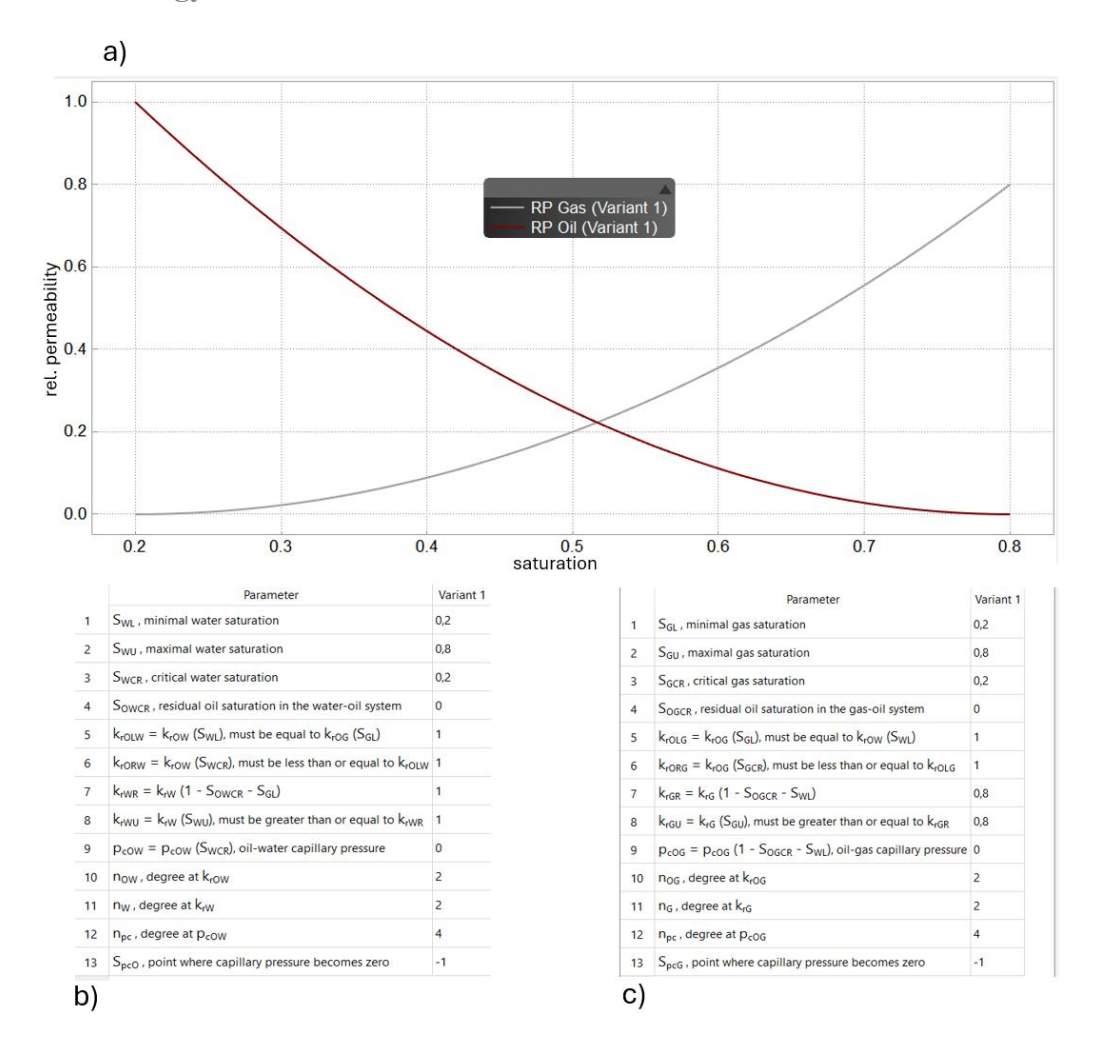


Figure 13 a) relative permeabilities curve b) corey exponent oil c) corey exponent gas

Corey-type functions are adopted for relative permeability estimation. Figure 13 b) report the data of Corey correlation for relative permeability curve of oil-water while Figure 13 c) the ones for gas-water. Some of this input data were kept as given by default from the simulator, the one changed were row1, 2, 3, 7, 8, 10 and 11 where the Corey exponents were modified from 4 to 2. The adjustment was necessary for the curvature of relative permeabilities curves to better aligned with the expected reservoir behaviour.

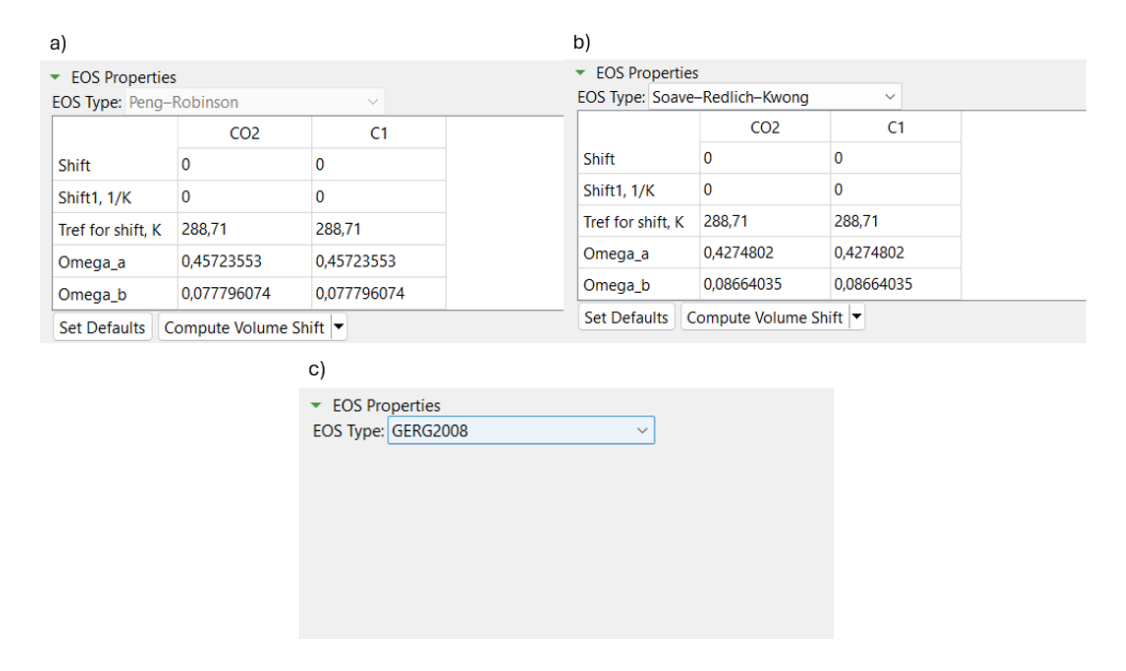


Figure 14 EOS Default parameters a) RKS b) PR c) GERG 2008

Each scenario described in Table 2 was simulated using the three different EOS models chosen for this study. This means that every scenario was run three times—once for each EOS. Each run generated slightly different results that were then collected for comparison and analysis.

Figure 15 lists the default parameters used for each EOS throughout all the simulations. Note that these standard parameters were used without any EOS Tuning.

For the Soave-Redlich-Kwong (SRK) and Peng-Robinson (PR) models, the software interface shows the characteristic parameters, such as  $\Omega_a$ ,  $\Omega_b$ , and the reference temperature for volume shift (Tref).

However, for the GERG-2008 EOS, these individual parameters are not displayed. This is because the GERG model works with a large, internal database that already contains the necessary interaction coefficients and physical constants for common types of gas mixtures. Because of this, the GERG-2008 model does not require the user to manually enter or adjust any settings, which helps to ensure that all simulations are both consistent and accurate.

# 4.2 Material Balance Analysis

The estimation of original gas-in-place (GOIP) is strongly related to the determination of the reservoir's pore volume. This process, in a first phase without production data, integrates diverse datasets, primarily including well logs, core analyses, bottom-hole pressure (BHP) measurements, and well test results. This information is synthesized to construct subsurface geological maps, such as structural and stratigraphic cross-sections, which are essential for delineating the

reservoir's areal extent and identifying geological discontinuities like faults, pinchouts, or fluid contacts [34].

Based on this geological framework, isopach maps are created to represent the reservoir's thickness. The Gross bulk volume is then computed by planimetering the areas enclosed between isopach contours, using numerical integration techniques like the trapezoidal or pyramidal rule [34]. The volumetric equation serves as a fundamental tool for quantifying GIP at any stage of reservoir depletion and for pre-production phase is used to estimate the Gas originally in Place (GOIP).

$$GOIP = \frac{GBV \cdot NTG \cdot \Phi \cdot (1 - S_{wi})}{BGi},$$
(4.1)

where GBV is the Gross Bulk Volume, NTG is the Net to Gross,  $\Phi$  is the porosity,  $S_{wi}$  the irreducible water saturation and BGi is the Formation volume factor for gas at initial conditions.

When a gas reservoir has an adequate production and pressure history, GOIP can be estimated without knowledge of volumetric parameters or initial water saturation  $S_{wi}$ . This is achieved by applying a material balance on the gas phase, which can be expressed as a molar balance. The fundamental principle states that the cumulative number of moles of gas produced is equal to the difference between the moles of gas initially present and the moles of gas remaining in the reservoir. This relationship is formulated as [34]:

$$N_p = N_i - N_f, (4.2)$$

where:

- $N_p$  = cumulative moles of gas produced
- $N_i$  = moles of gas initially in the reservoir
- $N_f$  = moles of gas remaining in the reservoir

Representing the gas reservoir by an idealized gas container, gas moles in Equation 4.2 can be replaced by their equivalents using the real gas law [16]:

$$PV = ZnRT, (4.3)$$

to give:

$$\frac{p_{sc}G_p}{T_{sc}} = \left(\frac{p_i}{z_i T}\right) V - \left(\frac{p}{z T}\right) V,\tag{4.4}$$

and solving for p/z gives:

$$\frac{p}{z} = \frac{p_i}{z_i} - \left(\frac{p_{sc}T}{T_{sc}V}\right)G_p. \tag{4.5}$$

Equation 4.5 is an equation of a straight line when p/z is plotted versus the cumulative gas production Gp, as shown in Figure 8. This straight-line relationship is perhaps one of the most widely used relationships for gas reservoir. The straight-line relationship provides the engineer with the reservoir characteristics:

- $slope = \frac{p_{sc}T}{T_{sc}V};$
- Intercept at Gp = 0 gives pi/zi;
- Intercept at p/z = 0 gives the gas originally in place;

• Cumulative gas production or gas recovery at any pressure.

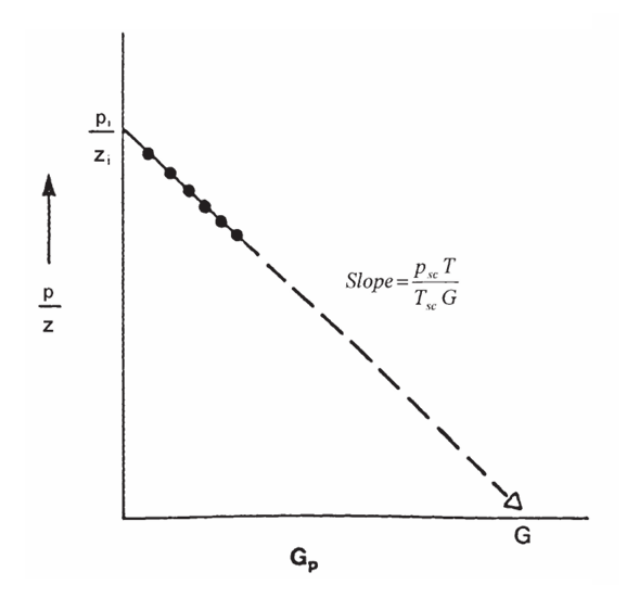


Figure 15 Gas material balance P/z [34].

The relationship between P/z and Gp is essentially linear. This popular equation indicates that by extrapolation of the straight line to abscissa, i.e., at p/z = 0, will give the value of the gas initially in place as Gp = GOIP.

In this study after the application of the method to the production phase, for the injection phase the p/z method was adapted for the evaluation of the max injectable gas at a given pressure and the results compared with the one of the simulator to estimate the precision of the result.

## 4.2.1 CCE-Based Estimation for the Production Phase

Being able to apply the material balance method p/z requires the compressibility factor Z. The gas compressibility factor is determined using a visual PVT cell that holds the reservoir fluid at its native temperature. This test provides the Z-factor for pressures at or above the saturation point. A key feature of this method is that the Z-factor only needs to be measured experimentally at a single pressure (p1). From this one measurement, its value at any other pressure (p) can then be calculated using equation 4.6[34]. In this study, thanks to the simulation of a Constant Composition Expansion (CCE) using the PVT Designer tool in t-Navigator, it was possible to estimate the Z-factor during the production phase for each time step, associated with the corresponding pressure points. This was possible due to the constant gas composition during depletion, consisting only of methane.

$$z = z_1 \left(\frac{p}{p_1}\right) \frac{V}{V_1} \tag{4.6}$$

## 4.2.2 Development of an Alternative Method for Injection

During the injection phase, it was not possible to assess the Z – Factor simulating a CCE test. The main reason is that the residual CH<sub>4</sub> in the reservoir, together with the increasing amount of injected gas, creates a gas mixture with a non-constant composition. These aspects make it not applicable for the calculation of the Z-factor during the injection phase.

This constraint led to develop an alternative method for the evaluation of the Z-factor during injection, to be able to perform the material balance analysis also for the injection data. Before applying this procedure to the injection data, it was tested on the production data, where both the Z-factor from the CCE output and the calculated Z-factor were available for comparison.

Assuming a constant molar mass equal to that of methane, the compressibility factor Z was calculated with a reformulation of the real gas law. In this form, the molar volume was substituted by the ratio of molar mass to density. The resulting expression is shown in Equation 4.7.

$$z = \frac{p \, MM}{R \, T \, \rho} \tag{4.7}$$

Considering that the compressibility factor equation contains density, another pressure dependent property, it was necessary to determine this parameter too. However, as for the *Z*-factor, it was not possible to retrieve it simulating a CCE test, therefore a different procedure has been followed. The density calculated at reservoir condition was estimated as follow:

$$Gas\ Density = \frac{Current\ Gas\ in\ Place\ (mass)}{Gas\ Original\ in\ Place\ (rm3)}. \tag{4.8}$$

The nominator "current gas in place (mass)" decreasing during production, remaining constant in shut in period and increasing in injection, represent the amount of gas mass in the reservoir. The denominator is the Original Gas in Place (volume), rm³ (reservoir condition). This value was chosen because it represents the total volume available to the gas, which is the correct physical quantity to use for calculating the gas mixture's density. As far as we know, no direct value was available for this initial gas volume at reservoir conditions. Therefore, the first value from the "displaced hydrocarbon in place" data column, which corresponds to the initial state before any production began, was used as the GOIP. Using these numerator and denominator values, Equation 4.8 allows for the calculation of the gas mixture's density at every pressure point

To evaluate the accuracy of each selected Equation of State —Peng-Robinson, Soave-Redlich-Kwong and GERG—in predicting the Z-factor and gas density, a statistical error analysis was performed. The experimental data from the Constant

Composition Expansion test were considered the benchmark values. First, the Absolute Percentage Error (APE) (Equation 4.9-4.10) was calculated for each data point predicted by the analytical calculation based on the data of the simulation, slightly different for each EOS, against the corresponding experimental value. Subsequently, the Mean Absolute Percentage Error (MAPE) was determined from the set of individual APEs to quantify the overall predictive accuracy of each EOS.

$$APE_Z = \left| \frac{Z_{\text{CCE}} - Z_{\text{analytical}}}{Z_{\text{CCE}}} \right| \tag{4.9}$$

$$APE_{\rho} = \left| \frac{\rho_{\text{CCE}} - \rho_{\text{analytical}}}{\rho_{\text{CCE}}} \right| \tag{4.10}$$

After validated, the methodology was applied to the injection data. For all the scenarios, the simulations were configured with consistent operational constraints to ensure a direct comparison of the results.

Following its validation, the method was applied to the CO<sub>2</sub> injection phase and H<sub>2</sub>. As the gas was a mixture of CH<sub>4</sub> and CO<sub>2</sub> or H<sub>2</sub>, it was necessary to calculate a mixture molar mass (MM mix) using Equation 4.11 and 4.12.

$$MM_{\text{mix}} = y_{CH_A} \cdot MM_{CH_A} + y_{CO_2} \cdot MM_{CO_2}$$
 (4.11)

$$MM_{\text{mix}} = y_{CH_4} \cdot MM_{CH_4} + y_{H_2} \cdot MM_{H_2}$$
 (4.12)

# 4.3 Computational cost Analysis

To provide a more in-depth analysis of the different EOS models and to better evaluate their cost-benefit trade-offs, this work includes an analysis of their computational performance. Several different metrics were used for this evaluation, beginning with the Total Calculation Time, referring to the actual real-world time elapsed from the beginning to the end of a simulation, also known as wall-clock time. This value includes all computational tasks and any input/output operations, essentially measuring how long the program runs. In contrast, Total GPU Time represents the cumulative time the graphics processing unit was actively performing calculations [39]. A Graphics Processing Unit (GPU) is a processor specifically designed to handle many operations in parallel, making it more efficient than a standard CPU for complex mathematical tasks. In this study, an NVIDIA GeForce RTX GPU was used to speed up the simulations. The Total GPU Time accounts for the GPU's full operational time, including both the core parallel computations and any data transfer between the CPU and the GPU [40]. This metric is valuable for understanding how effectively the GPU hardware was used. Another key metric is the CPU Time per Timestep, which measures the average CPU processing time needed to advance the simulation by a single time increment. This provides insight

into the computational effort required for each step. The simulations in this study use an implicit solver that relies on Newton iterations to solve the nonlinear governing equations at each timestep. Newton's method works by repeatedly simplifying (linearizing) a nonlinear problem to find a solution that meets a specific convergence criterion. This means that each timestep in the simulation may require several Newton iterations before the solution is considered final. A higher number of iterations increases the workload for the CPU, leading to a higher CPU Time per Timestep [41].

By analysing these metrics together, it is possible to understand how the computational work is divided between the CPU and GPU. For example, when the heavy mathematical calculations within each Newton iteration are moved to the GPU, the Total GPU Time will capture this parallel work, which can reduce the overall wall-clock time. The CPU Time per Timestep then highlights the remaining tasks handled by the CPU, such as managing the iterations. Ultimately, using these metrics allows for the identification of the characteristic of the model as precision and computational cost respect fast and lighter calculation paying in accuracy.

# **Chapter 5 Results and Analysis**

Once the simulations were run, the results were collected for analysis. In this chapter, we present both data directly obtained from tNavigator and results derived from analytical calculations.

# 5.1 Production Phase Analysis.

#### 5.1.1 EOSs Performance

In all the scenarios, the first phase is methane production, during which the reservoir is depleted until a recovery factor equal to 80% is reached. Figure 16 shows the corresponding pressure versus time for a production rate of 1,000,000 Sm³/day of methane. The simulator keeps the production rate constant until the pressure approaches the lower limit of 50 bar. The point at which the production rate changes, and so when the pressure tends to the imposed limit, depends on the Equation of State used.

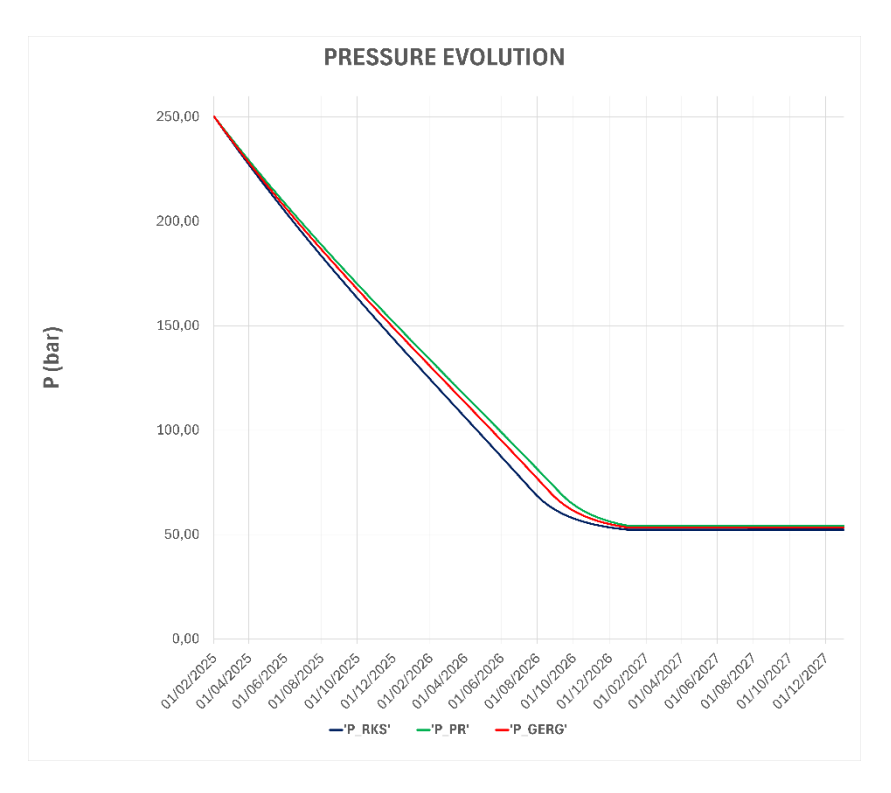


Figure 16. Comparison of pressures vs time for different EOSs during production phase.

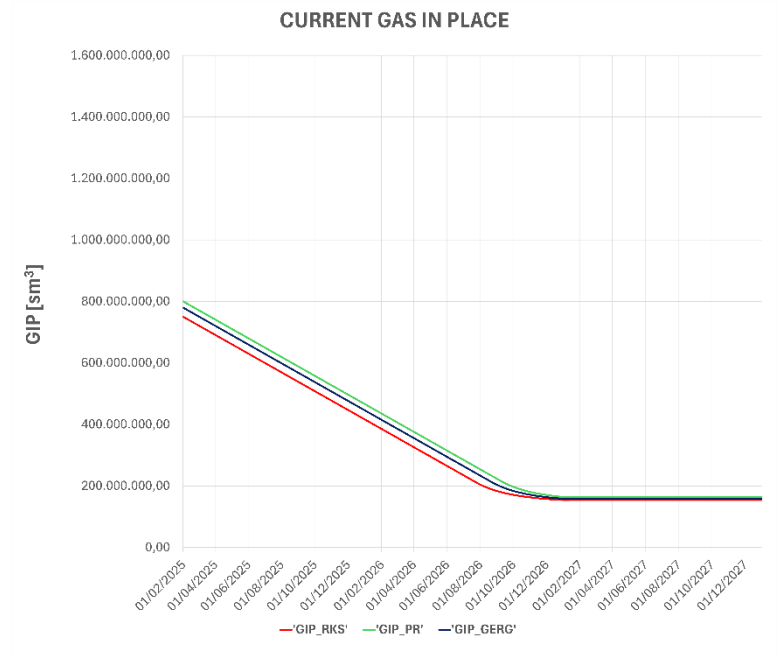


Figure 17 Current Gas in place Comparison

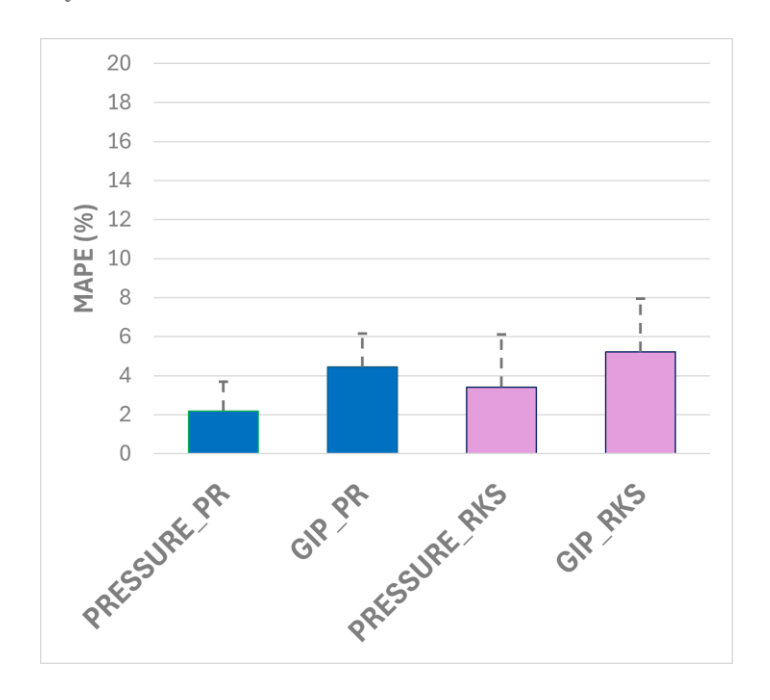


Figure 18 EOS error analysis Production

An analysis of the simulation outputs reveals that all three EOS models predict consistent trends for both reservoir pressure and gas depletion. We selected the GERG model to serve as the reference for accuracy, as it provides a realistic intermediate case between the other two models. As depicted in the results, the PR model exhibits a tendency to slightly overestimate pressure trend (Figure 16) and the remaining gas volumes (Figure 17) that match with the compressibility factor underestimation (Figure 19). In contrast, the RKS model predicts slightly lower pressures (Figure 16) and, lower gas in place, a behaviour that can be attributed to its simplified thermodynamic modelling. These findings are confirmed by the MAPE values, which show that the PR model aligns very closely with the GERG reference, whereas the RKS model introduces slightly higher deviations.

As described in the methodology section, the analytical method was validated by comparing the density and Z-factor values obtained using the analytical method proposed, with the outputs of the CCE tests. Figures 19 and 20 show respectively the Z-factor values obtained from the CCE test and the ones calculated using Equation 4.7, while the density values are reported in Figures 21 and 22

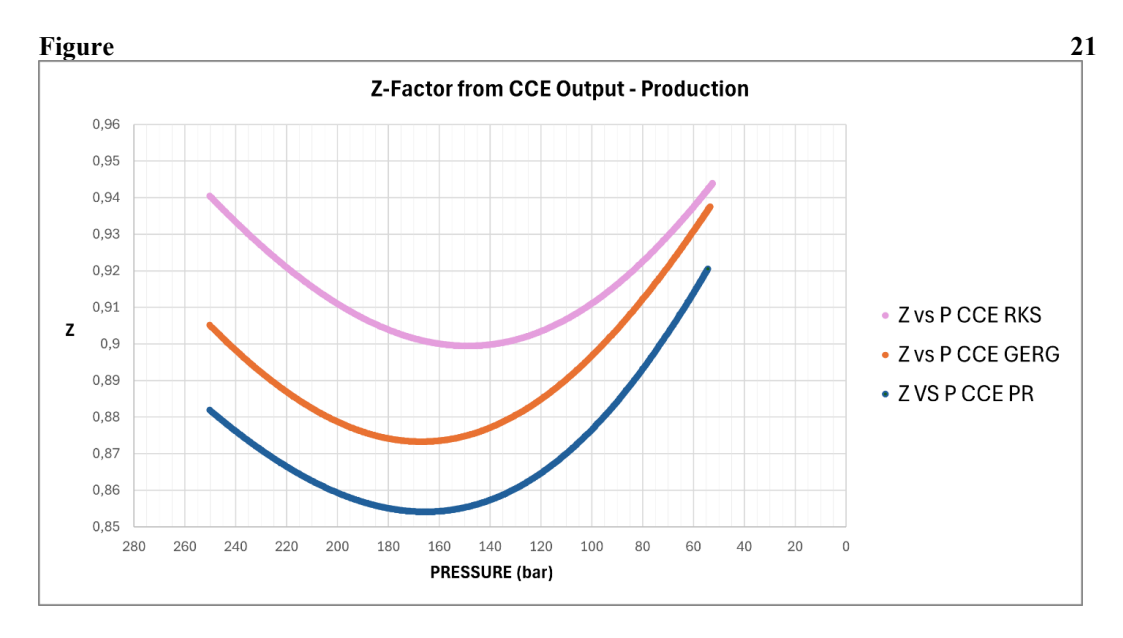


Figure 19. Z-Factor values from CCE output.

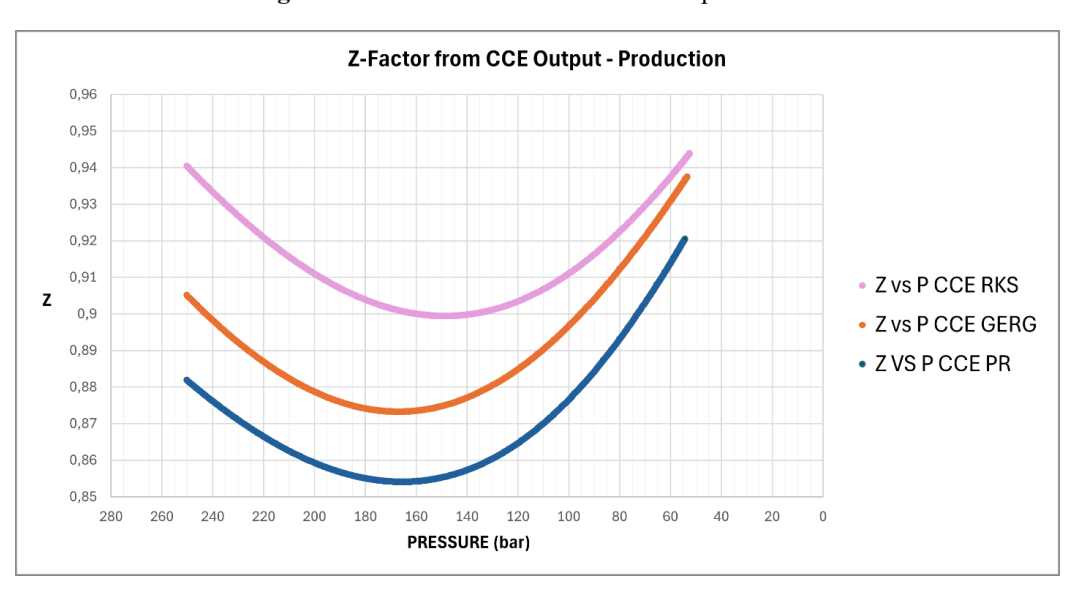


Figure 20. Z-Factor values calculated with Equation

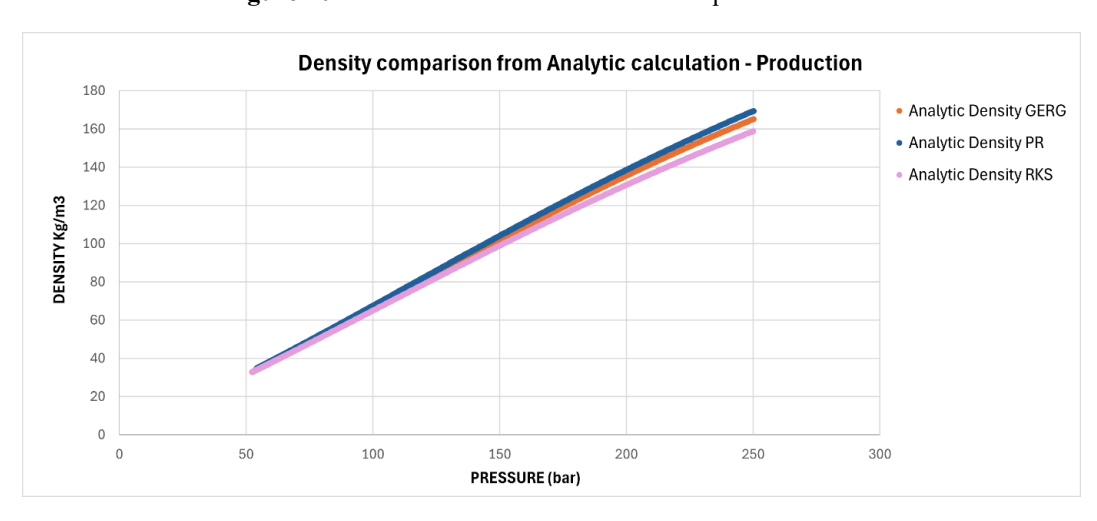


Figure 21. Densities in production phase calculated with equation

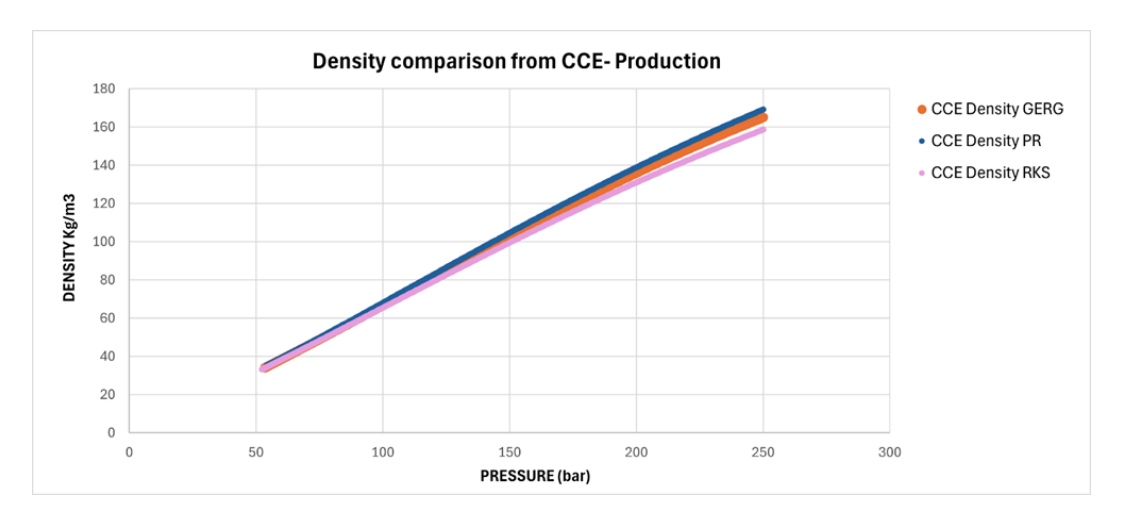


Figure 22. Densities in production phase retrieved from CCE experiment simulation.

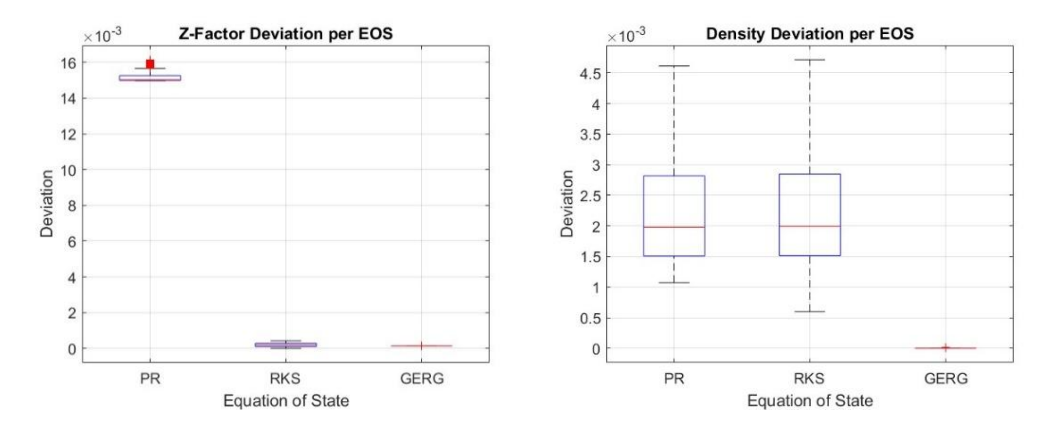


Figure 23. (A) Error deviation for Z-Factor. (B) Error deviation for Density.

A comparison of the results reveals excellent agreement between the analytical method (Figure 19 and 21) and the CCE simulations (Figure 20 and 22), with very low deviations observed both visually and through quantitative analysis (Figure 23). As expected, the GERG model provides the most accurate thermodynamic description. In comparison to the result of GERG also PR and RKS models exhibit low discrepancies between analytical and simulated data; PR shows a slightly higher deviation in the order of  $1.5 \times 10^{-4}$  MAPE in the Z-factor calculations, while for densities PR and RKS are both around  $2 \times 10^{-3}$  MAPE. These differences, however, are minimal and fall within acceptable error margins, thus validating the application of the analytical method for predicting real-gas properties during the injection phase.

## 5.1.2 Material Balance Analysis

The P/Z method was used to evaluate the Gas Original In Place for each EOS. The Z-factor used in the P/Z calculations was obtained from the PVT designer module,

using data from the CCE experiment simulated. The results are shown in Figure 24 and 25 and summarized in tables 3 and 4 respectively considering volumes and mass.

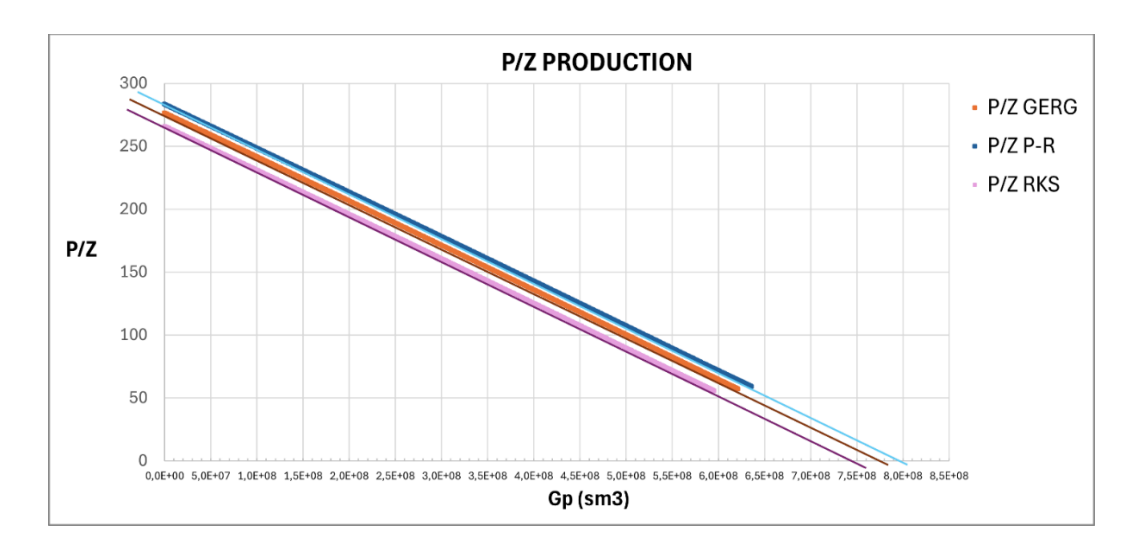


**Figure 24**. Comparison of GOIP in volume with P\Z method for different EoS during production phase.

**Table 3**. GOIP in mass form P\Z from different EOS.

EOS	GERG	P-R	RKS
P\Z GOIP [Sm3]	7,70E+08	7,90E+08	7,40E+08

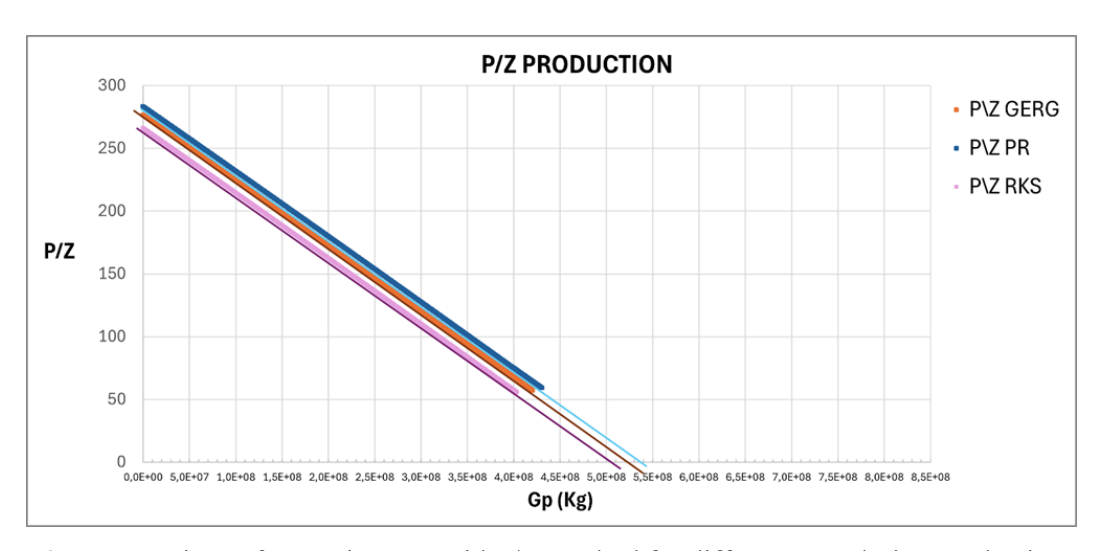


**Figure 25**. Comparison of GOIP in mass with P\Z method for different EoS during production phase.

Table 4 GOIP in mass form P\Z from different EOS.

EOS	GERG	P-R	RKS
P\Z GOIP [Kg]	5,25E+08	5,40E+08	5,00E+08

To validate the accuracy of the material balance method in estimating GOIP the MAPE with respect to the values obtained by the simulator was calculated.

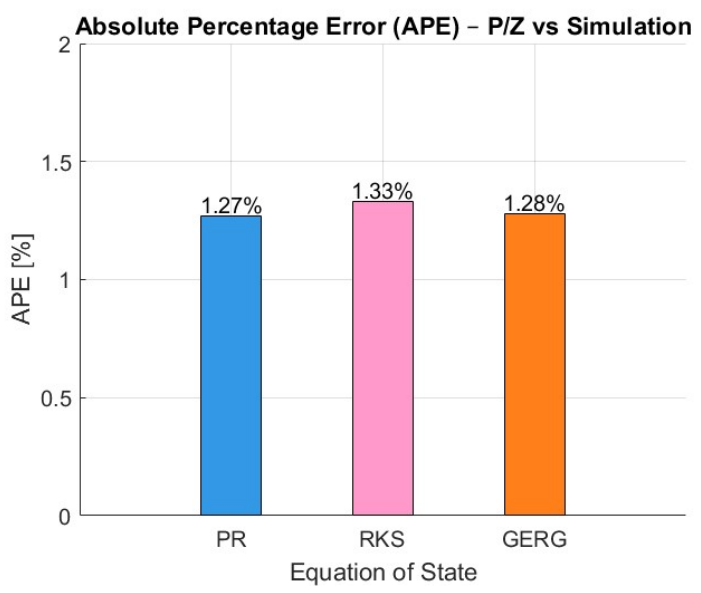


**Figure 26**. Comparison of GOIP in volume from P\Z and simulator during production phase.

The application of the P/Z method, which used pressure-dependent Z-factors derived from the CCE-based PVT model of each EOS, produced linear P/Z trends that allowed for a robust extrapolation to estimate the GOIP. On a volumetric basis, the analysis yielded GOIP values of  $7.9 \times 10^8 \, \mathrm{Sm^3}$  for PR,  $7.7 \times 10^8 \, \mathrm{Sm^3}$  for GERG, and  $7.4 \times 10^8 \, \mathrm{Sm^3}$  for RKS. This ranking was preserved for the mass-based estimates, which were  $5.4 \times 10^8 \, \mathrm{kg}$ ,  $5.25 \times 10^8 \, \mathrm{kg}$ , and  $5.00 \times 10^8 \, \mathrm{kg}$ , respectively. These discrepancies are directly attributable to systematic shifts in the Z-factor among the models: a lower Z-factor, as predicted by PR, increases the y-intercept and results in a higher GOIP, while a higher Z-factor from RKS decreases it. A quantitative comparison with the simulator results confirms the excellent agreement of this method, with Absolute Percentage Error values of 1.27% (PR), 1.28% (GERG), and 1.33% (RKS). These findings confirm the robustness of the P/Z approach and a following analysis on computational time will provide the data to evaluate the best balance cost accuracy.

# 5.2 CO<sub>2</sub> Injection Phase Analysis

#### 5.2.1 EOSs Performance

After the depletion phase, a stream of pure  $CO_2$  is injected into the reservoir with a rate equal to 1,000,000 Sm³/day. The final reservoir pressure is set to match the initial pressure, prior to production phase ( $P_{final} = P_{initial}$ ). The simulator keeps the injection rate constant until the pressure approaches this limit. Both the evolution of the injection rate and the pressure in the reservoir prior to the injection differ according to the EOS used.

**Using** the analytical method, the density and Z-factor were calculated for the injection phase.

Figure 30 shows the calculated densities, and Figure 31 shows the *Z*-factor values.

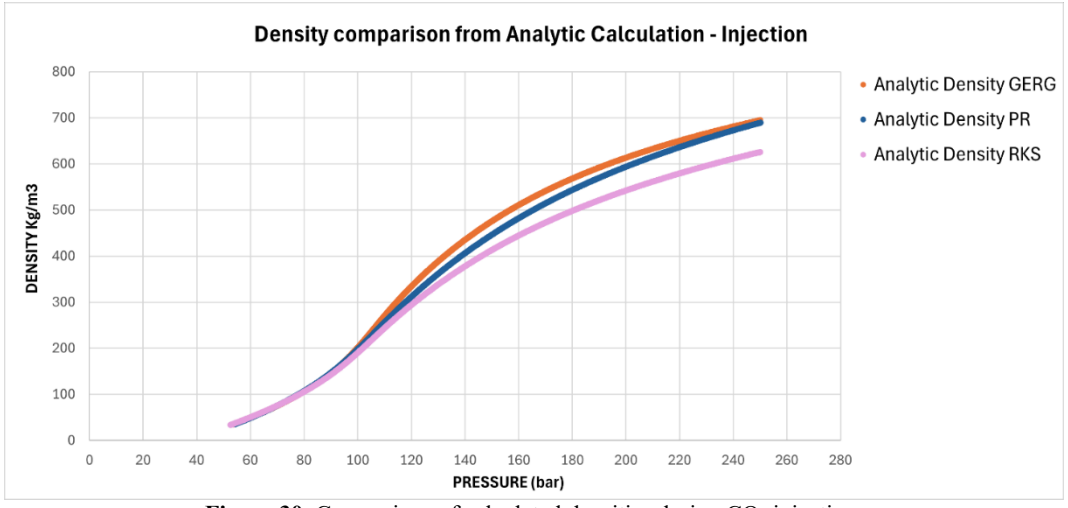


Figure 30. Comparison of calculated densities during CO2 injection.

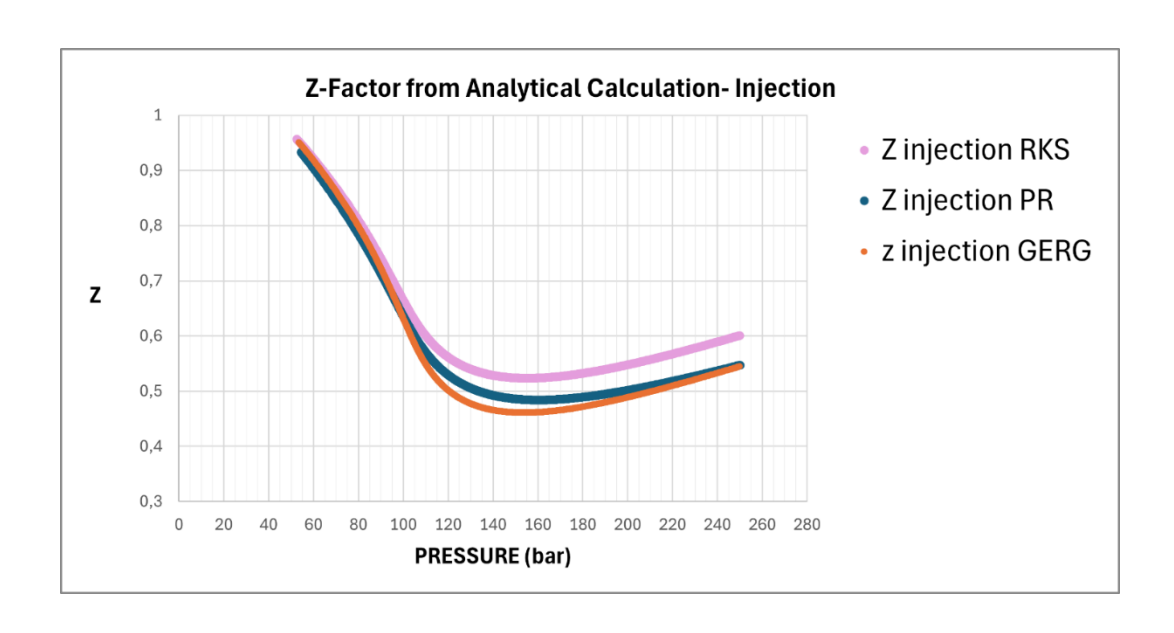


Figure 31. Z-Factor from analytical calculation during CO<sub>2</sub> injection.

The distinctions between the EOS models become more apparent during the injection phase. This happens because the gas mixture's behaviour deviates further from ideality as pressures increase, which makes the precise modelling of its thermodynamic properties especially important.

At the beginning of the injection process, all three EOS models provide nearly identical predictions, as shown by the overlapping initial segments of the pressure (Figure 27) and GIP curves (Figure 28) while from the beginning of 2029 at pressures slightly above 100 bar the trends start to diverge significantly. The GERG and PR models calculate very similar Z-factors (Figure 31) and densities (Figure 30). Consequently, their forecasts for both pressure buildup and cumulative gas-inplace are almost the same. The data curves for these two models remain closely matched for most of the injection period. In the final stages, PR displays a slight tendency to predict a higher pressure, overestimating it by less than 2% (Figure 29), which can be seen as a marginally steeper slope on the pressure evolution graph. In contrast, the RKS model, with its simpler formulation, consistently predicts higher Z-factors (Figure 31) and lower densities (Figure 30). This combination reflects a gas that is less compressible and lighter, which leads to two clear effects visible in the graphs. First, it results in a faster and more significant pressure build up for the same injected volume, as shown by its higher trajectory on the pressure plot. Second, it produces slightly higher volumetric storage estimations, which is reflected in the GIP plot where the RKS line sits just above the others toward the end of the injection. These consistent deviations underscore how sensitive injection performance forecasts are to the thermodynamic model of the gas mixture.

Figure 27. Comparison of pressures vs time for different EOSs during Co2 injection phase.

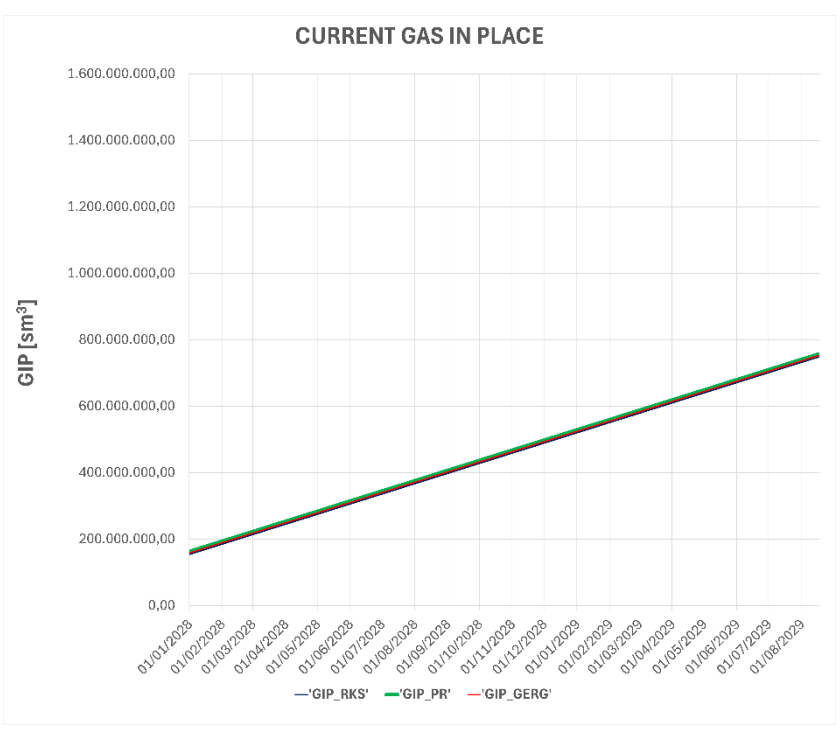


Figure 28 Current Gas in place Comparison

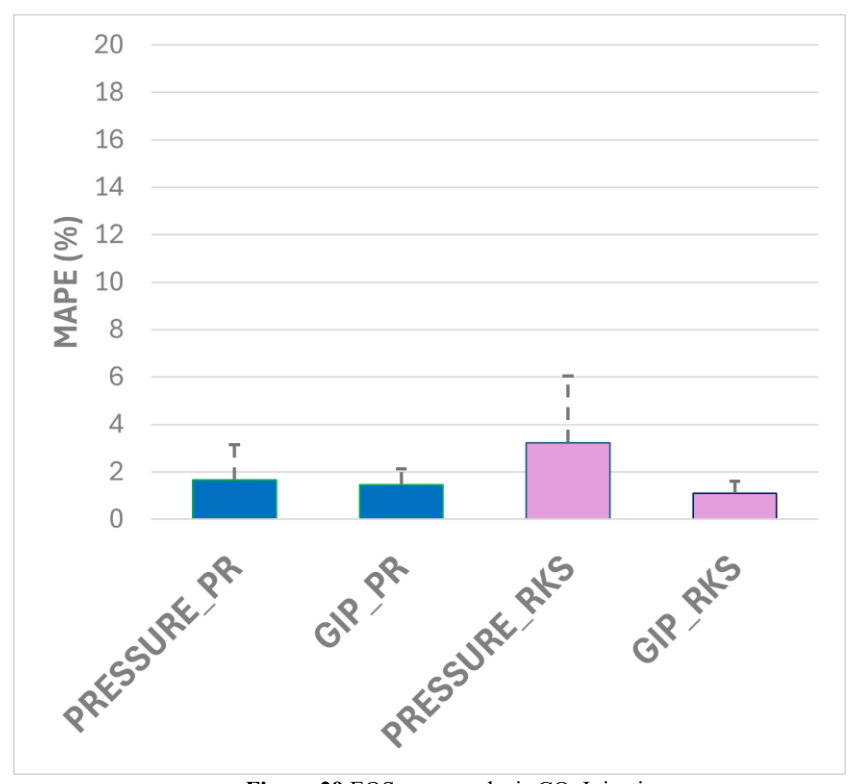


Figure 29 EOS error analysis CO2 Injection

Using the analytical method, the density and Z-factor were calculated for the injection phase.

Figure 30 shows the calculated densities, and

Figure 31 shows the *Z*-factor values.

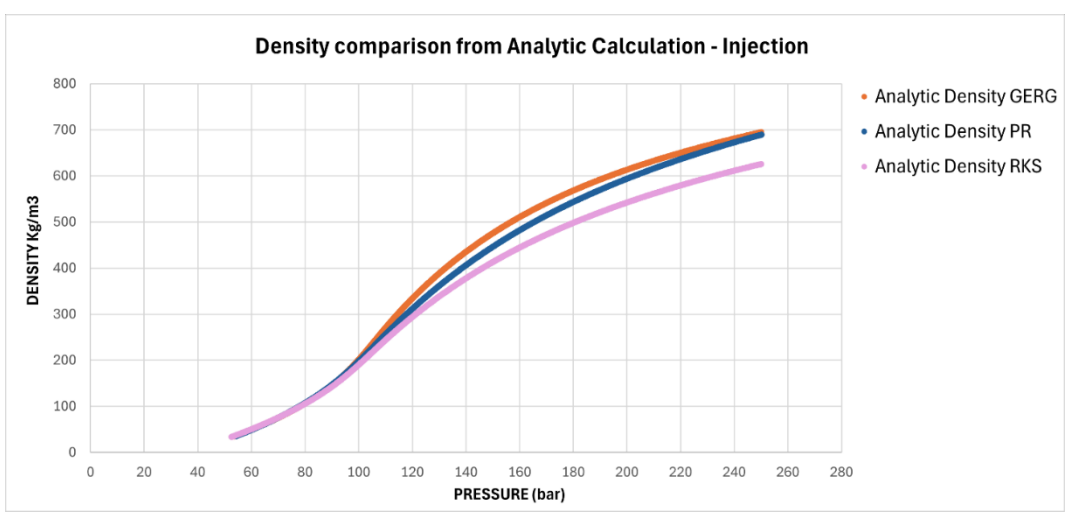


Figure 30. Comparison of calculated densities during CO2 injection.

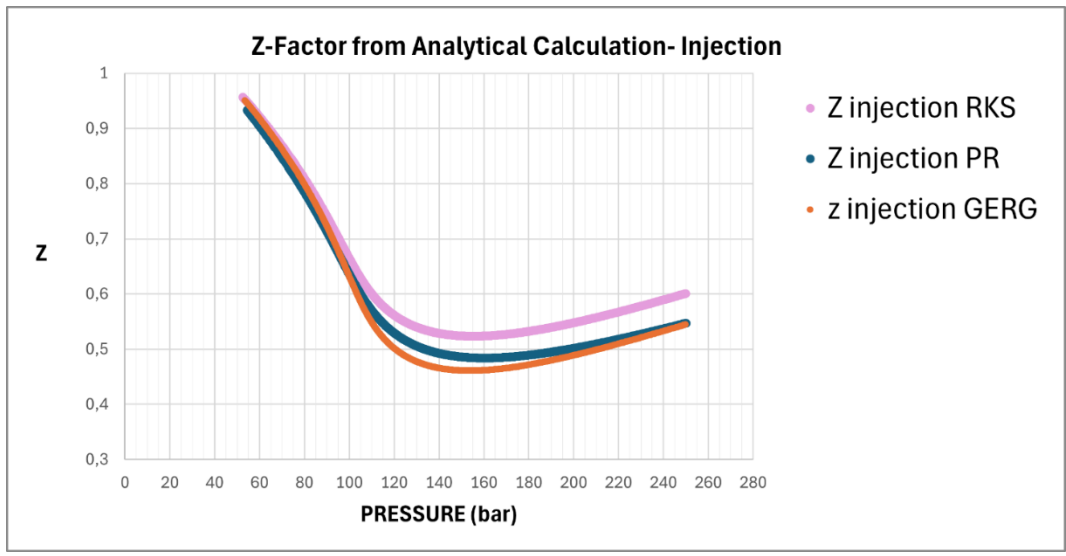


Figure 31. Z-Factor from analytical calculation during CO<sub>2</sub> injection.

The distinctions between the EOS models become more apparent during the injection phase. This happens because the gas mixture's behaviour deviates further from ideality as pressures increase, which makes the precise modelling of its thermodynamic properties especially important.

At the beginning of the injection process, all three EOS models provide nearly identical predictions, as shown by the overlapping initial segments of the pressure (Figure 27) and GIP curves (Figure 28) while from the beginning of 2029 at pressures slightly above 100 bar the trends start to diverge significantly. The GERG and PR models calculate very similar Z-factors (Figure 31) and densities (Figure 30). Consequently, their forecasts for both pressure buildup and cumulative gas-in-place are almost the same. The data curves for these two models remain closely matched for most of the injection period. In the final stages, PR displays a slight tendency to predict a higher pressure, overestimating it by less than 2% (Figure 29), which can be seen as a marginally steeper slope on the pressure evolution graph.

In contrast, the RKS model, with its simpler formulation, consistently predicts higher Z-factors (Figure 31) and lower densities (Figure 30). This combination reflects a gas that is less compressible and lighter, which leads to two clear effects visible in the graphs. First, it results in a faster and more significant pressure build up for the same injected volume, as shown by its higher trajectory on the pressure plot. Second, it produces slightly higher volumetric storage estimations, which is reflected in the GIP plot where the RKS line sits just above the others toward the end of the injection. These consistent deviations underscore how sensitive injection performance forecasts are to the thermodynamic model of the gas mixture.

## 5.2.2 Material Balance Analysis

Similarly to what has been done with the production phase data, the P/Z values for the injection phase are estimated using the Z-factors obtained from the analytical method. Since during the injection phase the P/z values increase as gas is progressively injected, to maintain the characteristic shape of the material balance plot observed during the production phase, the y-axis was inverted. Below the plots of P/Z in both volume and mass during the injection phase are reported.

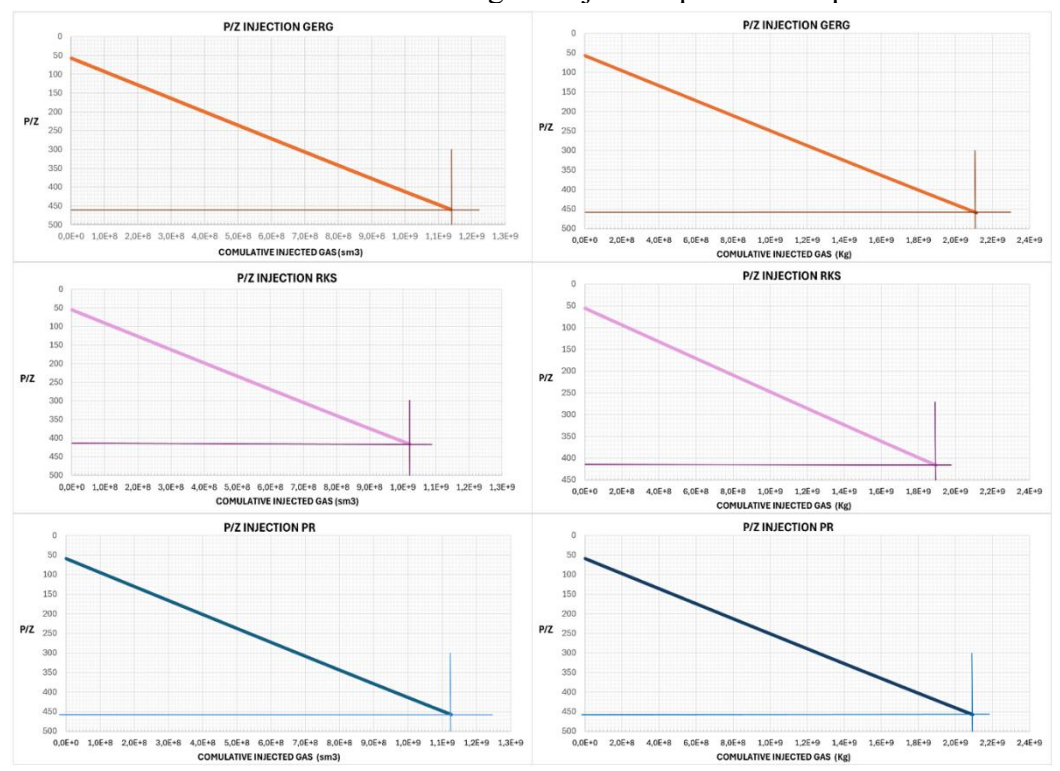


Figure 32 Matherial balance comparison.

For the interpretation of this data, our approach is to identify the final P/Z value corresponding to the maximum injection pressure reached. The corresponding value on the x-axis represents the maximum gas in place achievable at that pressure.

45

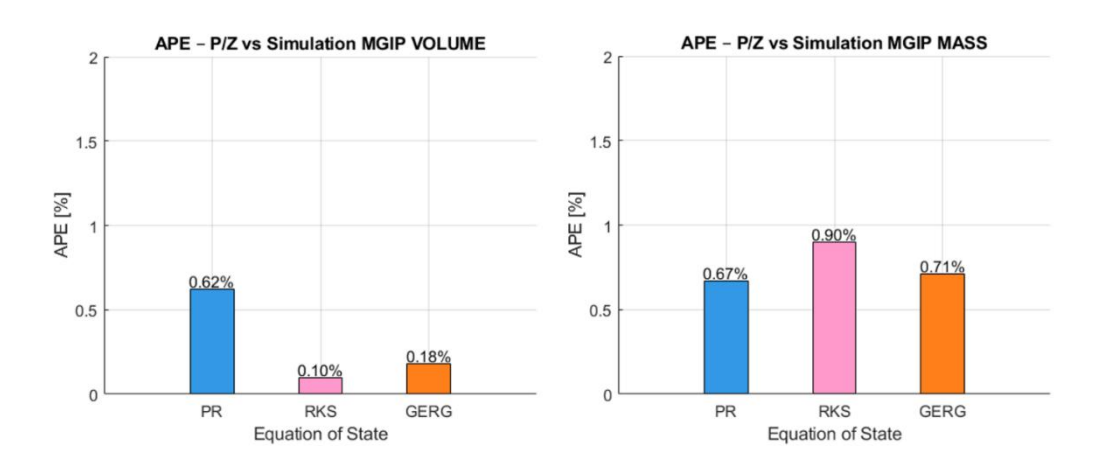


Figure 33 Absolute Percentage Error (APE) Between P/Z Method and Simulator Results for C02 Injection

At the end of the injection phase, the results for stored gas show clear distinctions among the three equations of state. When looking at the stored volume (Figure 33), GERG predicts a maximum of 1.15×10° Sm<sup>3</sup>, while both PR and RKS estimate a slightly larger capacity of around 1.20×10° Sm<sup>3</sup>. When comparing the stored mass, however, this trend is reversed. GERG calculates the highest injected mass at 2.10×10° kg, with PR's result being nearly identical at 2.09×10° kg. In contrast, RKS predicts a significantly lower mass of 1.90×109 kg. These differences are a direct result of how each EOS models gas properties under high-pressure conditions. The GERG model treats the gas as being more compressible and having a higher density. This property means that a larger amount of mass can fit into the same available pore space, which is the reason GERG calculates the highest stored mass while reporting the lowest standard volume. In contrast, the RKS model, simulate the gas as less compressible and not as dense. As a result, it tends to slightly overestimate the potential storage volume but underestimate the actual mass that is stored. PR functions as a model in between the other two; its volume prediction is very similar to that of RKS, while its mass prediction is nearly identical to GERG's. The high accuracy of the analytical P/Z method, when checked against the detailed tNavigator® simulation, is confirmed by the two bar charts in Figure 34. As seen in the left chart for the volume comparison, the Absolute Percentage Error is very low for every model: RKS has the smallest error at 0.10%, followed by GERG at 0.18%, and PR slightly higher at 0.62%. This demonstrates that the P/Z method can accurately reproduce volumetric gas-in-place values. For the mass comparison (right chart), the errors also remain below 1%, proving the method's reliability even when considering density changes. GERG and PR perform very similarly, with APEs of 0.71% and 0.67%, while RKS has a slightly higher error of 0.90%, reflecting its lower accuracy in predicting densities. Overall, the low APE values for both volume and mass confirm that the analytical P/Z approach is a robust and accurate tool for estimating the maximum gas-in-place during injection, regardless of the chosen EOS. This validates its usefulness for assessing storage

performance while also showing how the choice of thermodynamic model predictably influences the results.

## **5.2.3** Computational cost

The three additional graphs in this section provide a look at the computational performance of each EOS during the injection phase. These plots show how the complexity of a model impacts the speed and stability of the simulation. The GERG model requires the most computational effort. The CPU time needed for each timestep varies significantly, with noticeable spikes, particularly as the injection progresses. This is due to GERG's complex formulation, which increases the solver's workload as system pressure rises. By the end of the simulation, its total calculation time is more than four times that of RKS. These variations suggest the solver must take smaller steps or perform more iterations to ensure a stable solution. The PR model is more efficient, with a stable CPU time per timestep and only small fluctuations. Its total runtime is much lower than GERG's, while still providing a comparable level of accuracy, as shown by the earlier P/Z and APE results. This confirms PR as a good balance between precision and computational cost, making it a suitable choice for large-scale studies. RKS is the fastest model, showing a consistently low and stable CPU time. However, this speed comes at the cost of accuracy. As discussed previously, its simplified gas modelling leads to less precise results, such as overestimating storage volume while underestimating the actual stored mass. In conclusion, while GERG is the most physically accurate, it is computationally expensive. PR achieves nearly the same accuracy with a much lower computational cost and better stability, making it the most practical option. RKS is useful for quick preliminary studies where speed is the priority, but its limitations must be considered. This shows that selecting an EoS has a major impact on both the storage predictions and the overall efficiency of the reservoir simulation.

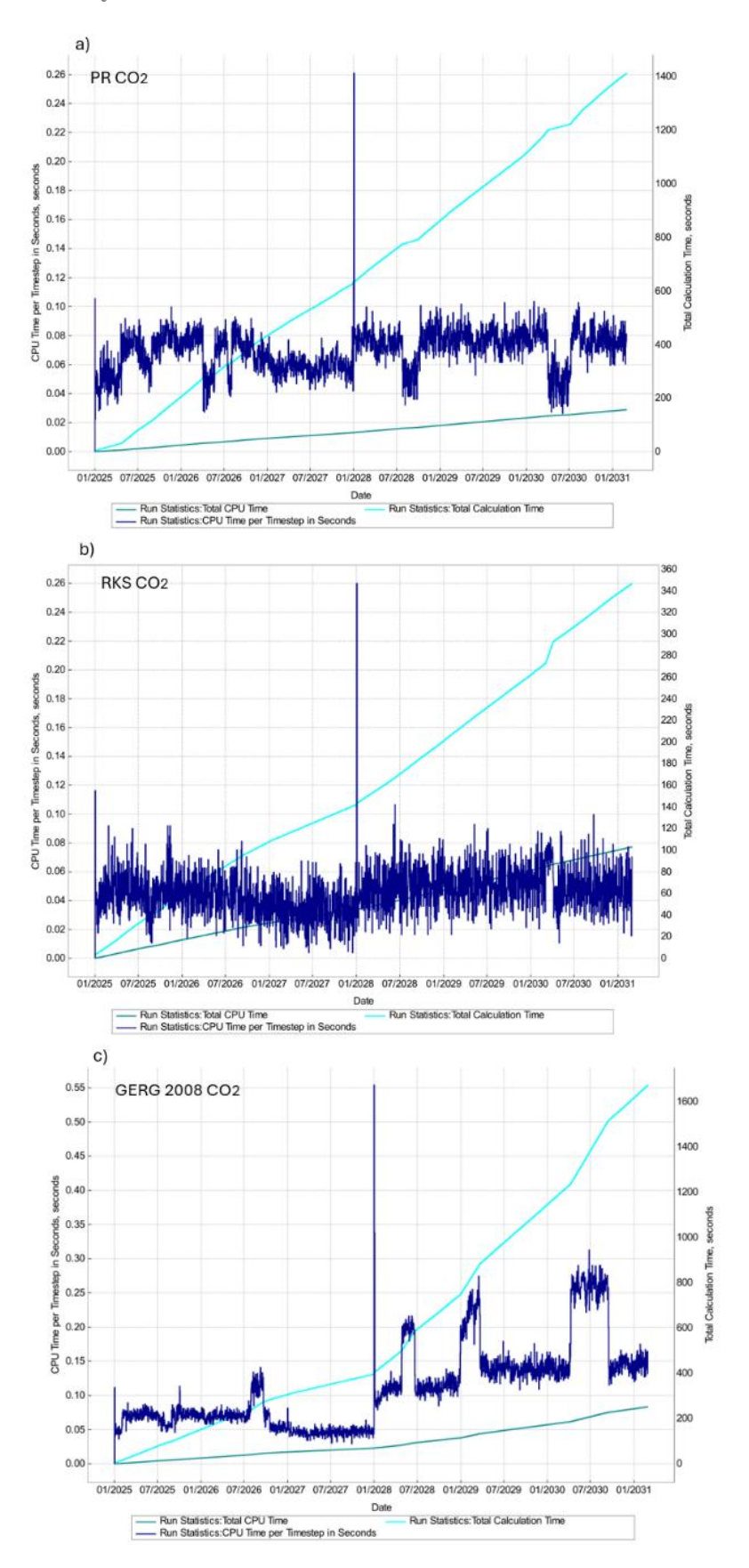
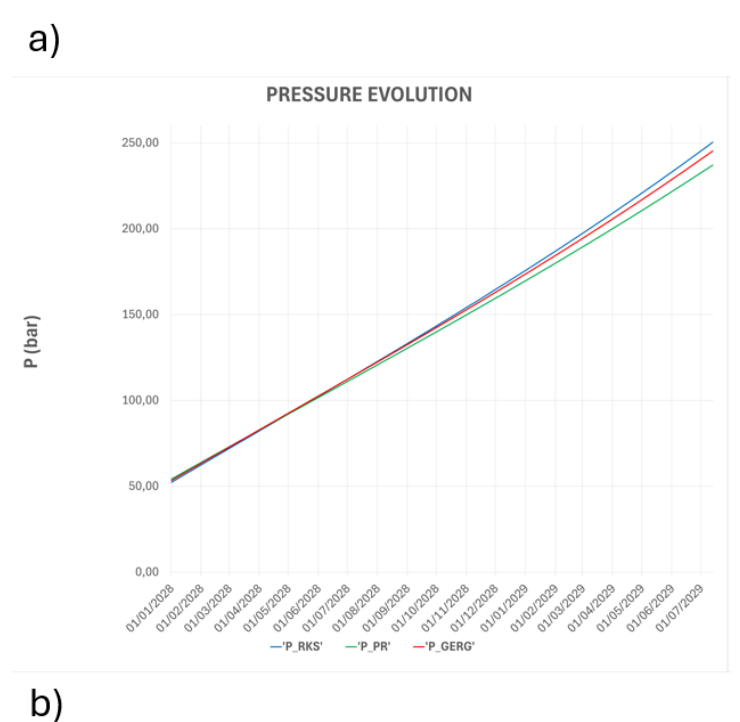


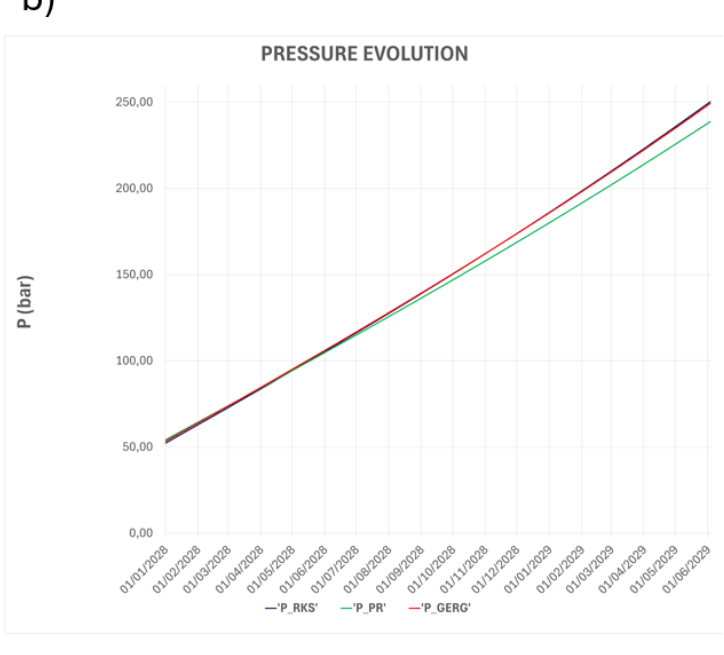
Figure 34 Computational costs for CO2 injection a) PR b) RKS c) GERG

# 5.3 H<sub>2</sub> Injection Phase Analysis

#### 5.3.1 EOSs Perfomance

The simulation results show the reservoir's response for the different H<sub>2</sub>-CH<sub>4</sub> Injection scenario described in table 2. As the molar concentration of hydrogen increases, the time required to reach the 250 bar pressure limit decreases. This is because the lower density and different compressibility of hydrogen allow for faster pressure build-up at the same volumetric injection rate. The pressure evolution for each scenario is shown in the figures below.





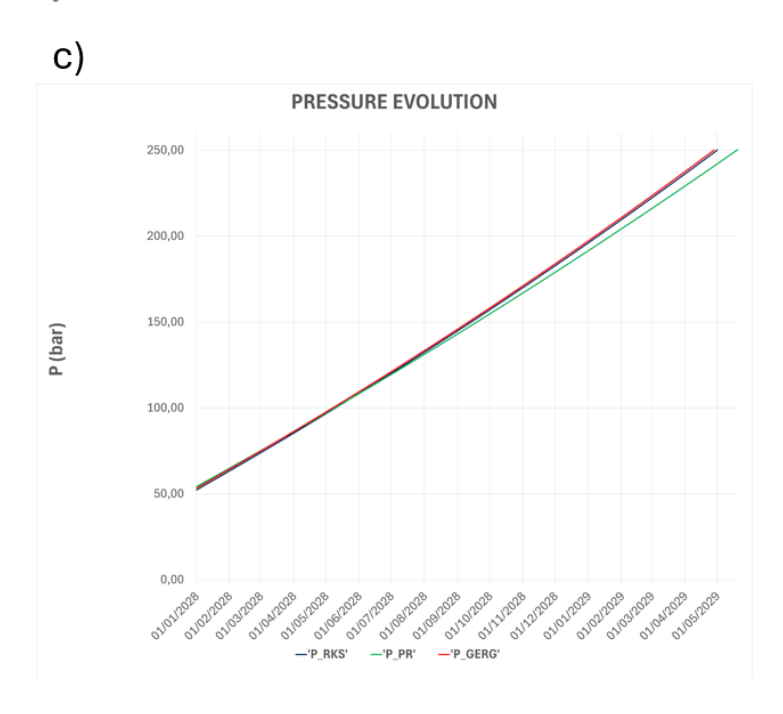


Figure 35 Comparison of pressures vs. Time for different EOS during all H2 injection scenario a) H2 20% b) H2 50% c) H2 100%

Table 5 Pressure vs time for different EOS and Injection scenario

H2 20%	PR	RKS	GERG
Final pressure	250,24	250,36	250,13
Days of injection	594	559	571
H2 50%	PR	RKS	GERG
Final pressure	250	250,34	250,4
Days of injection	547	519	505
H2 100%	PR	RKS	GERG
Final pressure	250,4	250,15	250,15
Days of injection	505	486	483

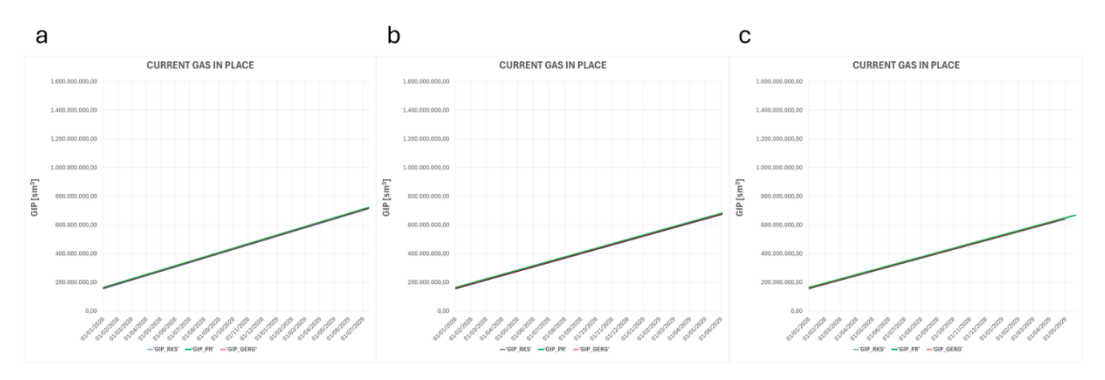


Figure 36 Current Gas in place comparison a) H2 20% b) H2 50% c) H2 100%

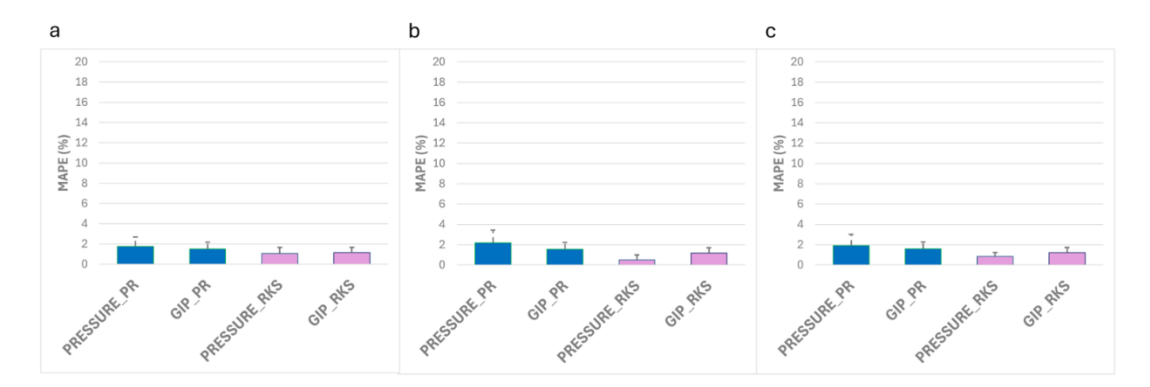


Figure 37 EOS Error Analysis a) H2 20% b) H2 50% c) H2 100%

Applying the analytical method, the gas density and Z-factor were calculated for the hydrogen injection scenarios. Figure 38 shows the calculated gas density as a function of pressure. A higher concentration of hydrogen results in a substantially lower mixture density due to its low molar mass.

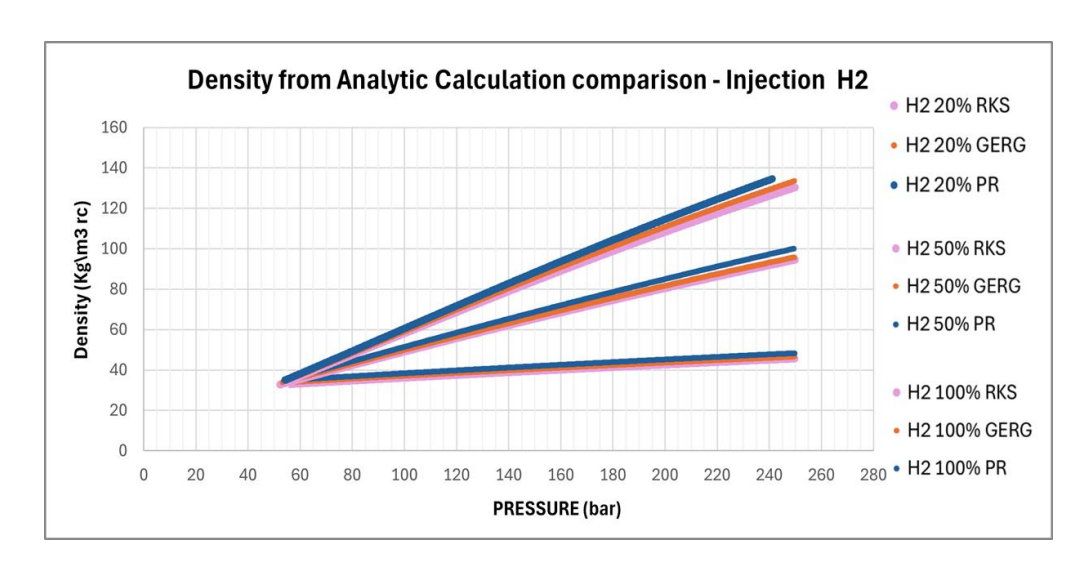


Figure 38. Comparison of calculated densities for H<sub>2</sub> injection.

The graphs below display the calculated Z-factor values for each scenario. In the cases with 100% and 50% H<sub>2</sub>, the Z-factor shows a steady and continuous increase as pressure rises. However, the 20% H<sub>2</sub> scenario, which has a high concentration of methane, behaves differently. Its curves first decrease to a minimum point before they start to rise, which is a typical trend for methane-rich gases.

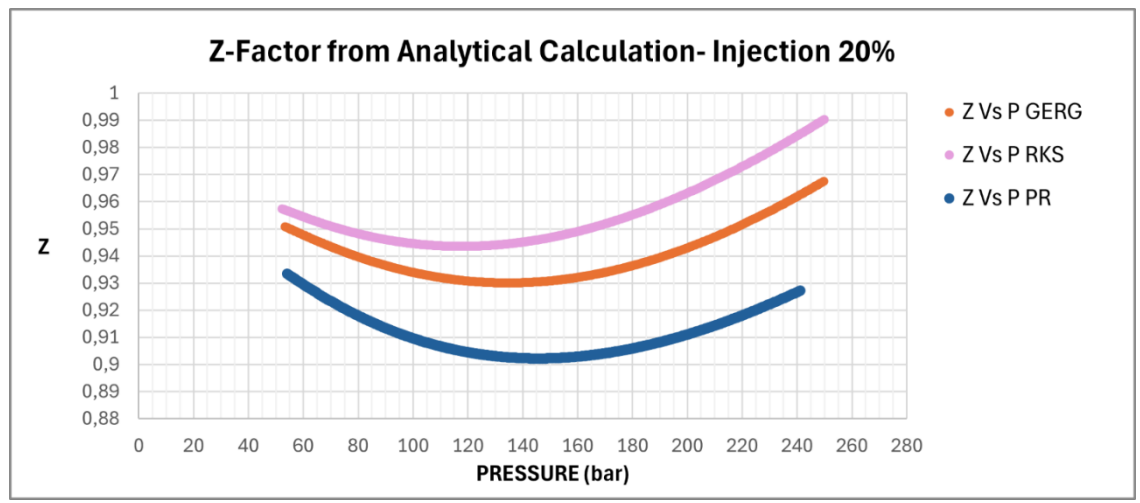


Figure 39. Calculated Z-Factor for the 20% H<sub>2</sub> scenario.

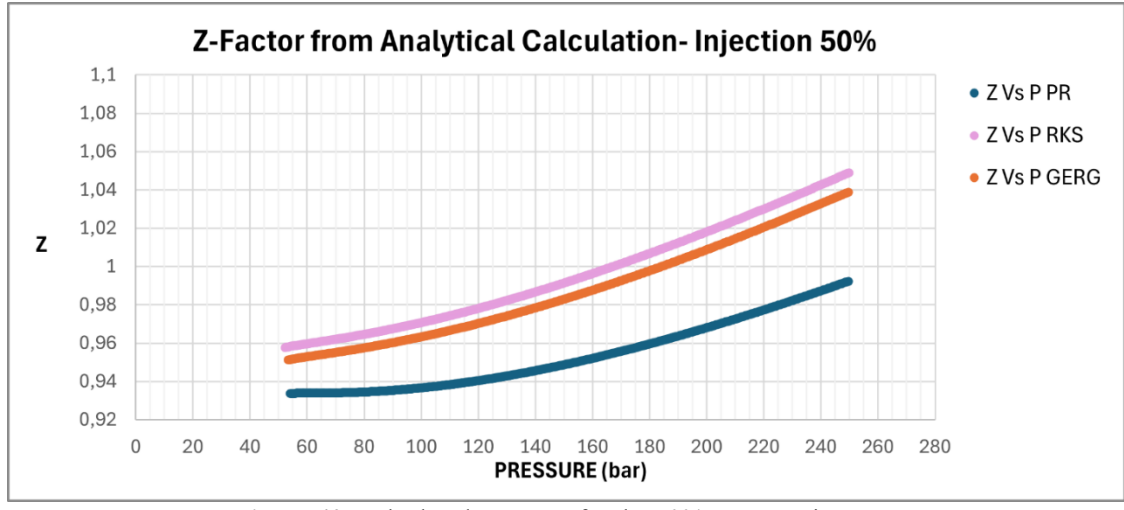


Figure 40. Calculated Z-Factor for the 50% H<sub>2</sub> scenario.

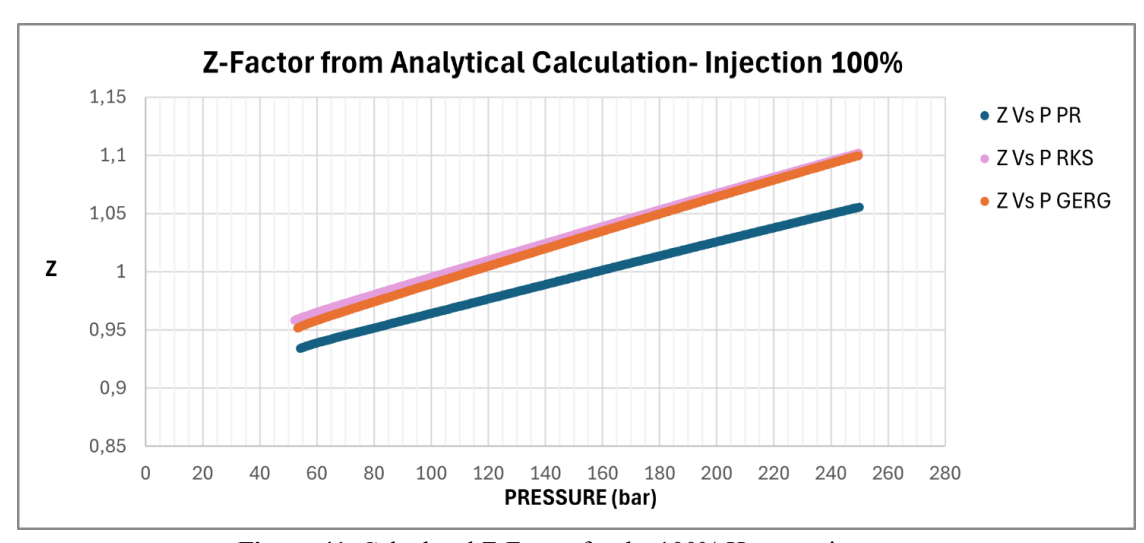


Figure 41. Calculated Z-Factor for the 100% H<sub>2</sub> scenario.

These Z-factor values are then used as inputs for the P/Z material balance analysis of the hydrogen injection phase.

At a higher hydrogen concentration of 50%, the differences between the EOS models become more distinct. In the pressure chart (Figure 35 b)), the PR curve is the one that separates from the others, while the predictions from RKS and GERG remain very close to each other. This behaviour corresponds to the Z-factor plot for the 50% mixture (Figure 40), which shows PR having the lowest value, indicating a more compressible gas. RKS has the highest Z-factor, and GERG is in the middle. The density chart for this mixture (Figure 38) shows the reverse of this trend, with the ranking being PR, followed by GERG, and then RKS.

Toward the end of the injection period, a clear separation in the volumetric Gas-in-Place predictions was not seen. The PR model forecasts the highest stored volume, while GERG and RKS predict a slightly lower, nearly identical volume. The Mean Absolute Percentage Error (Figure 37 b)) for pressure shows a moderate increase, with the largest error seen for PR, as expected since its curve is the one that diverges. In contrast, the GIP errors for all models remain low.

For the pure hydrogen (100% H<sub>2</sub>) scenario, the previously observed pattern continues and becomes more pronounced. In the pressure versus time plot (Figure 35 c)), the PR model's prediction clearly separates from the other two, while the curves for RKS and GERG remain closely grouped together. An analysis of the Z-factor for 100% H<sub>2</sub> (Figure 41) shows that PR has the lowest value, RKS has the highest, and GERG's value is very near to that of RKS. Although the overall gas densities are lower in this pure hydrogen case (Figure 38), the ranking among the models is consistent: PR predicts the highest density, followed by GERG, and then RKS. The Gas-in-Place curves continue to show a linear trend. Once again, PR calculates the largest volumetric GIP, while the predictions from RKS and GERG are almost identical to each other and slightly lower. The Mean Absolute Percentage Error values are all low (Figure 37 c)), staying below a few percent. The error in

the pressure forecast is primarily due to the divergence of the PR model, whereas the GIP errors remain minimal for all three EOS.

# **5.3.2** Material Balalce Analysis

To provide a detailed quantitative validation, Figure 42 consolidates the Absolute Percentage Error (APE) between the Maximum Gas in Place derived from the P/Z method and the final injected gas quantities reported by the simulator. The figure is organized by H<sub>2</sub> concentration (20%, 50%, and 100%), with separate plots illustrating the error for both the volumetric (Sm<sup>3</sup>) and mass (kg) comparisons.

**Table 6 .** Comparison of MGIP in mass and volume for different EOS during all H2 injection scenario

H2 20%	PR	RKS	GERG
P/z Mass	3.3 E+08	3.1 E+08	3.2 E+08
P/z Volume	3.65 E+08	5.55 E+08	5.7 E+08
H2 50%	PR	RKS	GERG
P/z Mass	2.10 E+08	1.95 E+08	1.98 E+08
P/z Volume	5.45 E+08	5.15 E+08	5.18 E+08
H2 100%	PR	RKS	GERG
P/z Mass	4.30 E+07	4.15 E+07	4.10 E+07
P/z Volume	5.00 E+08	4.80 E+08	4.80 E+08

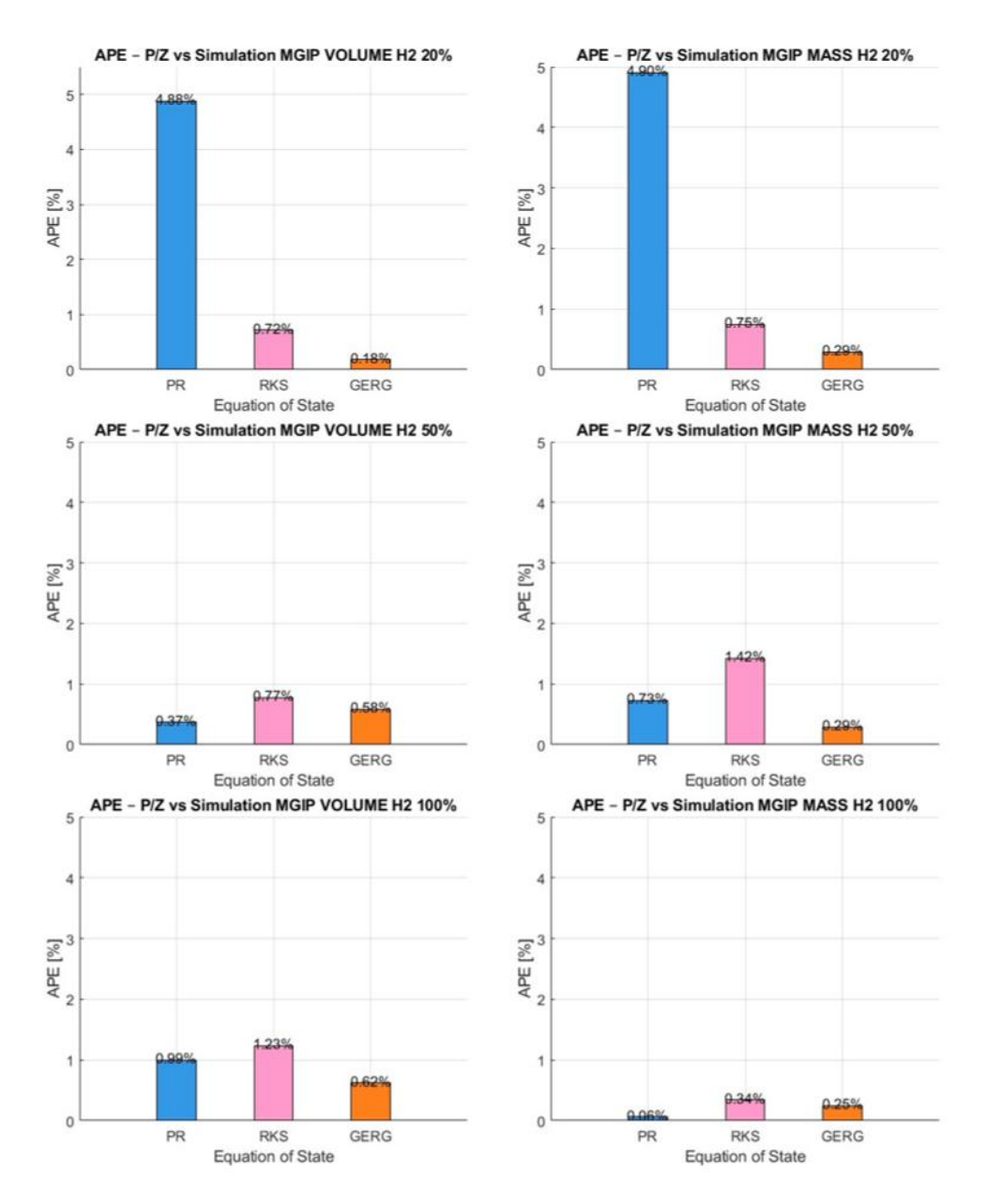


Figure 42 APE Analysis

When looking at Table 6, the overall pattern is simple. For the stored mass, PR always predicts the most, RKS predicts the least, and GERG is in the middle. This pattern holds true for all hydrogen concentrations, from 20% to 100%. For the stored volume, there is one important change to note. At 20% H<sub>2</sub>, PR calculates the smallest volume, while GERG and RKS are higher. However, from 50% H<sub>2</sub> and up, PR begins to predict the largest volume, with GERG and RKS following closely behind it.

This change makes sense based on the properties of the gas mixtures. As more hydrogen is added, the gas has a higher Z-factor and a lower density. This causes

the total mass that can be stored to go down for all EOS models. PR, which calculates the lowest Z-factor and highest density of the three, starts to predict the largest volume once the mixture becomes rich in hydrogen.

Regarding accuracy, the analytical P/Z method matches the simulator results well in almost all situations. The only clear exception is the PR model at 20% H<sub>2</sub>, where a consistent error appears. At 50% and 100% H<sub>2</sub>, the agreement gets even better for all EOS models. GERG is generally the most consistent, and PR is particularly accurate at predicting the mass when using 100% H<sub>2</sub>.

# 5.3.3 Computational cost

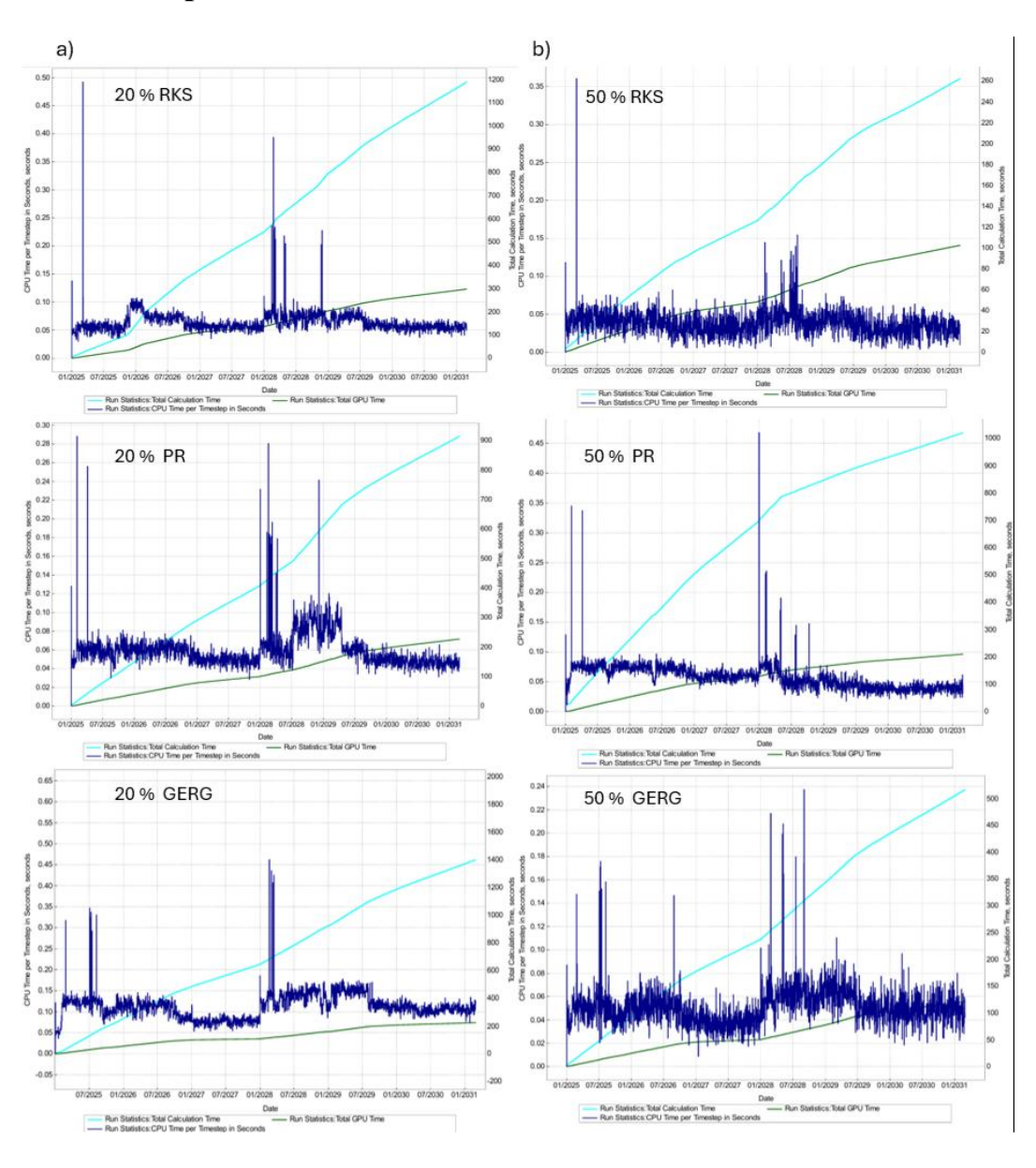
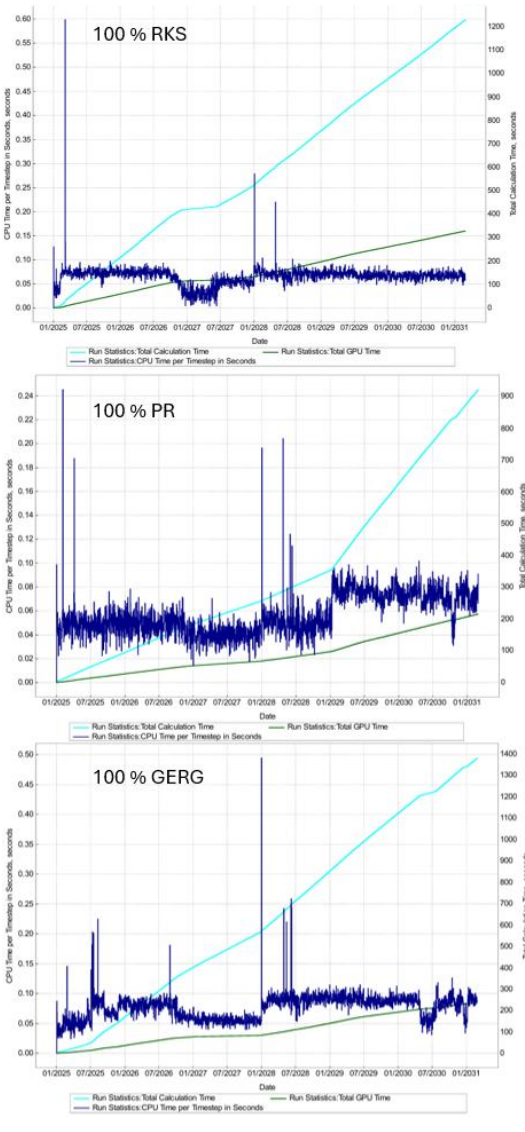


Figure 43 Computational costs for H2 injection a) 20% b) 50% in molar fraction



**Figure 44** Computational costs for H<sub>2</sub> injection at 100% molar fraction

The data on simulation run times shows a clear and consistent pattern (Figure 43 and 44). RKS is always the fastest model. Its calculation time for each step is the most stable, and it has the shortest total run time. This speed is a result of its simple formulas, but this is also the reason for the small errors mentioned earlier. GERG is slower but still reliable. It has more frequent spikes in calculation time, yet it always manages to find a solution, and its accuracy is always high.

PR's speed is between that of RKS and GERG when using 20-50% H<sub>2</sub>. However, it becomes the slowest model at 100% H<sub>2</sub>. This is because its predictions of a lower Z-factor and higher density make the calculations more difficult for the simulator in high-pressure, hydrogen-rich conditions. The simulator has to do more work and sometimes take smaller steps to find a solution, which increases both the time per step and the total run time.

Putting it all together, if speed is the most important factor, RKS is the best choice. If accuracy is the top priority, GERG is the safest model to use as a

reference. For a balanced option, especially at 50-100% H<sub>2</sub>, PR predicts the largest storage capacity and matches the simulator results very well. Its run time is longer than RKS's but remains at a manageable level

# Chapter 6 Conclusions

The analysis begins with the depletion phase, where all three Equations of State)—GERG-2008, Peng–Robinson, and Soave–Redlich–Kwong —predict very similar pressure declines and gas production volumes. This indicates that for single-phase conditions, the choice of EOS has a minor effect on the results. However, small but consistent differences are present and correspond to how each model handles realgas behaviour. PR tends to calculate lower Z-factors, leading to slightly higher pressures and remaining gas. RKS produces higher Z-factors and slightly lower pressures and Gas-in-Place (GIP). GERG's predictions fall between the two matching his role of reference for accuracy. The P/Z plots are linear in all cases, and the Gas-Originally-in-Place (GOIP) calculated from the P/Z method is very close to the simulator's value, with minimal errors.

During CO<sub>2</sub> injection, the gas behaves less ideally, and the differences between the EOS models become larger but remain explainable. For these plots, the Z-factor was determined using the analytical method. The pressure buildup and stored gas predictions for PR and GERG remain very similar, meaning they calculate comparable Z-factors and densities within the relevant pressure range. RKS continues to show a higher Z-factor and lower density. As a result, the injected gas appears less compressible and lighter, causing pressure to rise more quickly at the same surface injection rate. In practical terms, GERG tends to show a greater mass stored at a given pressure, PR provides nearly the same accuracy as GERG with a shorter runtime, and RKS is suitable for initial screening but is less precise.

With hydrogen injection, these differences become stronger, and a clear trend related to composition appears. As the H<sub>2</sub> concentration increases from 20% to 100%, the Z-factor rises, and density falls for all models. This causes the pressure to increase faster and reduces the mass that can be stored per unit of pore volume. At 20% H<sub>2</sub>, the models are still very similar, though PR's pressure curve begins to separate slightly. At 50% H<sub>2</sub> and higher, the separation is clear: PR gives the largest volume and mass, while GERG and RKS remain closely grouped with slightly

#### **Conclusion**

lower values. The P/Z method remains accurate across all H<sub>2</sub> scenarios, with errors generally below one percent.

These results are a direct consequence of how each EOS is designed. The simplicity of RKS makes it behave more like an ideal gas, pushing its Z-factor up and density down. GERG is based on a multi-fluid, Helmholtz-energy approach that best matches real gas data, making it a reliable benchmark.

Computationally, RKS is the fastest because its calculations are the simplest. GERG is the slowest, as its complex calculations require more time, especially at high pressures. PR generally offers the best balance between accuracy and speed.

Overall, three main points emerge. First, the P/Z method with an analytical Z-factor provides reliable storage estimates. Second, the choice of EOS leads to predictable differences in pressure and storage capacity. Third, there is a clear trade-off between precision and speed: GERG is the most accurate but also the most computationally demanding; PR is nearly as accurate and usually faster, making it the most practical choice; and RKS is best for quick initial estimates.

Next step for future work could be to test these models in more complex reservoirs with varied geological structures and active aquifer support. This would help determine not just how much accuracy is gained with a more advanced model like GERG, but also when that extra accuracy is worth the computational cost over a project's lifetime. This perspective links the choice of model to its economic impact, helping to balance accuracy and simulation time.

- [1] F. Proedrou, «A new framework for EU energy security: putting sustainability first», *Eur. Polit. Soc.*, vol. 18, fasc. 2, pp. 182–198, apr. 2017, doi: 10.1080/23745118.2016.1215374.
- [2] J. Rogelj *et al.*, «Paris Agreement climate proposals need a boost to keep warming well below 2 °C», *Nature*, vol. 534, fasc. 7609, pp. 631–639, giu. 2016, doi: 10.1038/nature18307.
- [3] R. Tarkowski, «Underground hydrogen storage: Characteristics and prospects», *Renew. Sustain. Energy Rev.*, vol. 105, pp. 86–94, mag. 2019, doi: 10.1016/j.rser.2019.01.051.
  - [4] «IMET-1991-250».
- [5] L. Vandermeer, «CO2 Storage in the Subsurface», in *Greenhouse Gas Control Technologies 6th International Conference*, vol. I, Elsevier, 2003, pp. 201–206. doi: 10.1016/B978-008044276-1/50032-5.
- [6] B. Wei, B. Wang, X. Li, M. Aishan, e Y. Ju, «CO2 storage in depleted oil and gas reservoirs: A review», *Adv. Geo-Energy Res.*, vol. 9, fasc. 2, pp. 76–93, ago. 2023, doi: 10.46690/ager.2023.08.02.
- [7] Lu, Y.; Tian, R.; Liu, W.; et al., «Mechanisms of shale water wettability alteration with chemical groups after CO<sub>2</sub> injection: Implication for shale gas recovery and CO<sub>2</sub> geostorage», vol. 90, 2021, doi: 10.1016/j.jngse.2021.103992.
- [8] V. A. Yartys e M. V. Lototsky, «An Overview of Hydrogen Storage Methods», in *Hydrogen Materials Science and Chemistry of Carbon Nanomaterials*, vol. 172, T. N. Veziroglu, S. Yu. Zaginaichenko, D. V. Schur, B. Baranowski, A. P. Shpak, e V. V. Skorokhod, A c. di, in NATO Science Series II: Mathematics, Physics and Chemistry, vol. 172., Dordrecht: Springer Netherlands, 2004, pp. 75–104. doi: 10.1007/1-4020-2669-2\_7.
- [9] Muhammed, N. S., Haq, B., Al Shehri, D., Al-Ahmed, A., Rahman, M. M., e Zaman, E., «A review on underground hydrogen storage: insight into geological sites, influencing factors and future outlook», *Energy Rep.*, vol. 8, pp. 461–499, 2022, doi: 10.1016/j.egyr.2021.11.166.

- [10] T. Huang, G. J. Moridis, T. A. Blasingame, A. M. Abdulkader, e B. Yan, «Compositional reservoir simulation of underground hydrogen storage in depleted gas reservoirs», *Int. J. Hydrog. Energy*, vol. 48, fasc. 92, pp. 36035–36050, nov. 2023, doi: 10.1016/j.ijhydene.2023.05.355.
- [11] Ali, A. A.; Elhassan, A. H.; Elameen, M. A.; Ahmed, A. A.; Musa, H, «Thermodynamic Behavior Description of a Reservoir Fluid by Using Cubic Equations of State», *Pet. Chem.*, vol. 64, fasc. 7, pp. 1–8, set. 2024, doi: 10.1134/S0965544124050074.
- [12] van der Waals, J. D., «van der Waals, J. D. 1913. The law of corresponding states for different substances. s.l.: KNAW, Proceedings, Vol. XV, 1913», *Law Corresp. States Differ. Subst.*, vol. Vol. XV, 1913.
- [13] I. G. Economou, «Cubic and Generalized van der Waals Equations of State», in *Applied Thermodynamics of Fluids*, A. R. Goodwin, J. Sengers, e C. J. Peters, A c. di, The Royal Society of Chemistry, 2010, pp. 53–83. doi: 10.1039/9781849730983-00053.
- [14] J. O. Valderrama, «The State of the Cubic Equations of State», *Ind. Eng. Chem. Res.*, vol. 42, fasc. 8, pp. 1603–1618, apr. 2003, doi: 10.1021/ie020447b.
- [15] O. Kunz e W. Wagner, «The GERG-2008 Wide-Range Equation of State for Natural Gases and Other Mixtures: An Expansion of GERG-2004», *J. Chem. Eng. Data*, vol. 57, fasc. 11, pp. 3032–3091, nov. 2012, doi: 10.1021/je300655b.
- [16] Poling, Bruce E, Prausnitz, John M., e O'Connell, John P., *The Properties of Gases and Liquids*, 5th ed. McGraw-Hill, 2001.
- [17] Bejan, e Adrian, *Advanced Engineering Thermodynamics*, 4th ed. Hoboken, NJ: John Wiley & Sons, 2016.
- [18] Pitzer, Kenneth S., «The Volumetric and Thermodynamic Properties of Fluids. I. Theoretical Basis and Virial Coefficients», *J. Am. Chem. Soc.*, vol. 77, fasc. 13, pp. 3427–3433, lug. 1955, doi: 10.1021/ja01619a010.
- [19] Schmidt, G.; Wenzel, H., «A modified van der Waals type equation of state», *Chem. Eng. Sci.*, vol. 35, pp. 1503–1512, 1980, doi: 0.1016/0009-2509(80)80045-2.
- [20] Daridon, J. L.; Lagourette, B.; Saint-Guirons, H.; Xans, P., «A generalized process for phase equilibrium calculation with cubic equations of state», *Int. J. Thermophys.*, vol. 14, pp. 949–961, 1993, doi: 10.1007/BF00502356.
- [21] Mathias, P. M., «A versatile phase equilibrium equation of state», *Ind. Eng. Chem. Process Des. Dev.*, vol. 22, fasc. 3, pp. 385–391, 1983, doi: 10.1021/i200022a020.
- [22] Mangold, F.; Lemmon, E. W.; Span, R, «equation of state and thermodynamic properties for mixtures of H<sub>2</sub>O, O<sub>2</sub>, N<sub>2</sub>, and CO<sub>2</sub> from ambient up to 1000 K and 280 MPa», *J. Supercrit. Fluids*, vol. 153, p. 104577, 2019, doi: 10.1016/j.supflu.2019.104577.

- [23] Twu, C. H.; Coon, J. E.; Cunningham, J. R., «A cubic equation of state with a new alpha function and a new mixing rule», *Fluid Phase Equilibria*, vol. 69, pp. 33–50, 1991, doi: 10.1016/0378-3812(91)85039-V.
- [24] Redlich, O.; Kwong, J. N. S, «Chemical Reviews», *Thermodyn. Solut. V Equ. State Fugacities Gaseous Solut.*, vol. 44, pp. 233–244, 1949, doi: 10.1021/cr60137a013.
- [25] Soave G., «Chemical Engineering Science», *Equilib. Constants Modif. Redl.-Kwong Equ. State*, vol. 27, fasc. 6, pp. 1197–1203, 1972, doi: 10.1016/0009-2509(72)80096-4.
- [26] Peng, D.-Y.; Robinson, D. B, «Industrial & Engineering Chemistry Fundamentals», *New Two-Constant Equ. State*, vol. 15, fasc. 1, pp. 59–64, doi: 10.1021/i160057a011.
- [27] Firoozabadi, Abbas, *Thermodynamics of Hydrocarbon Reservoirs*. New York: McGraw-Hill, 1989.
- [28] M. R. Riazi, *Characterization and properties of petroleum fractions*, 1st ed (Online-Ausg.). in ASTM manual series, no. MNL 50. West Conshohocken, Pa: ASTM International, 2005. doi: 10.1520/MNL50-EB.
- [29] Kunz, O.; Klimeck, R.; Wagner, W.; Jaeschke, M, «The GERG-2004 Wide-Range Equation of State for Natural Gases and Other Mixture», Gasund Wärme-Institut (GERG) / VDI Verlag Year: 2007, Düsseldorf, 2007.
- [30] E. W. Lemmon e R. Tillner-Roth, «A Helmholtz energy equation of state for calculating the thermodynamic properties of fluid mixtures», *Fluid Phase Equilibria*, vol. 165, fasc. 1, pp. 1–21, nov. 1999, doi: 10.1016/S0378-3812(99)00262-9.
- [31] P. Wang e G. A. Pope, «Proper Use of Equations of State for Compositional Reservoir Simulation Proper Use of Equations of State for Compositional Reservoir Simulation», 2001.
- [32] A. Kamashev e Y. Amanbek, «Reservoir Simulation of CO2 Storage Using Compositional Flow Model for Geological Formations in Frio Field and Precaspian Basin», *Energies*, vol. 14, fasc. 23, p. 8023, dic. 2021, doi: 10.3390/en14238023.
- [33] OpenGeoSys Developers, «Mathematical Formulation of the Black-Oil Model», OpenGeoSys Documentation. [Online]. Disponibile su: https://docs.opengosim.com/theory/mathematical\_formulation\_of\_black\_oil/
- [34] T. H. Ahmed, *Reservoir engineering handbook*, 3rd ed. Burlington, MA: Elsevier/Gulf Professional, 2006.
- [35] J. Moortgat e A. Firoozabadi, «Higher-Order Compositional Modeling in Three-Phase Flow in Porous Media», *SPE J.*, vol. 17, fasc. 3, pp. 788–797, 2012, doi: 10.2118/141268-PA.
- [36] Mathias, P. M., Klotz, H. C., e Prausnitz, J. M., «Fluid Phase Equilibria», *Equ.--State Mix. Rules Multicomponent Mix. Probl. Invariance*, vol. 67, 1991, doi: 10.1016/0378-3812(91)85033-P.

- [37] J. Lohrenz, B. G. Bray, e C. R. Clark, «Calculating Viscosities of Reservoir Fluids from their Compositions», *J. Pet. Technol.*, vol. 16, fasc. 10, pp. 1171–1176, 1964, doi: 10.2118/915-PA.
- [38] K. Bogachev, S. Milyutin, e A. Grishin, «A Dynamic Reservoir Modeling Approach Using the Gerg-2008 Equation of State for CCUS Projects», in *SPE Advances in Integrated Reservoir Modelling and Field Development Conference and Exhibition*, Abu Dhabi, UAE: SPE, giu. 2025, p. D011S002R003. doi: 10.2118/225333-MS.
  - [39] «Simulation Results: User Guide».
- [40] V. Yaneva-Cormack, «Accelerating Software Test Execution Using GPUs».
- [41] MOOSE Framework Team, «Solving Nonlinear Systems MOOSE Framework Documentation», MOOSE Framework. [Online]. Disponibile su: https://mooseframework.inl.gov